Journal of Fluids and Structures (1999) **13,** 723–754
Article No.: jfls. 1999.0231 available online at http://www.idealibrary.com on IDEAL

A NUMERICAL STUDY OF UNSTEADY FLUID FLOW IN IN-LINE AND STAGGERED TUBE BANKS

S. B. Beale

National Research Council of Canada, Montreal Road
Ottawa, Ontario K1A 0R6, Canada

AND

D. B. Spalding

Concentration Heat and Momentum Ltd., Bakery House, 40 High Street
Wimbledon, London SW19 5AU, U.K.

(Received 7 July 1998 and in revised form 19 March 1999)

This paper is concerned with the results of numerical calculations for transient flow in in-line-square and rotated-square tube banks with a pitch-to-diameter ratio of 2:1, in the Reynolds number range of 30–3000. Transient-periodic behaviour is induced by the consideration of two or more modules, with a sinusoidal span-wise perturbation being applied in the upstream module. There is a triode-like effect, whereby the downstream response to the stimulus is amplified, and there is a net gain in the crosswise flow component. When an appropriate feedback mechanism is provided, a stable transient behaviour is obtained, with alternate vortices being shed from each cylinder. Flow visualization studies of the results of the calculations are presented together with quantitative details of pressure drop, lift, drag and heat transfer. For the staggered bank, a wake-switching or Coanda effect was observed as the serpentine-shaped wake attached to alternate sides of the downstream cylinder. The induced response is independent of the amplitude and frequency of the applied disturbance, including the case of spontaneous behaviour with no excitation mechanism. For the in-line case where each cylinder is in the shadow of the previous one, the motion is less pronounced; however, a shear-layer instability associated with the alternating spin of shed vortices was observed. In this case, the response was found to be somewhat dependent on the frequency of the applied disturbance, and a transient motion could not be induced spontaneously in the absence of an explicit feedback mechanism. Calculated Strouhal numbers were in fair agreement with experimental data: for the staggered geometry, they had values of between 0·26 and 0·35, or from -21 to $+6\%$ higher than measured values, while for the in-line geometry, the Strouhal numbers ranged between 0·09 and 0·12, or about 20–40% lower than experimental values.

1. INTRODUCTION

1.1. General Background

Banks of plain tubes are often used in cross-flow heat exchanger designs, because they combine ease of construction with reasonable thermal and mechanical efficiency. Both in-line and staggered geometries are commonly employed. Although it was once maintained that there was insufficient space for vortices to develop in the passages of tube banks (Owen 1965; LeFeuvre 1973), the results of flow-visualization studies suggest that vortex shedding is present in tube banks, and that together with the phenomena of acoustic coupling and

0889–9746/99/060723 + 32 $30.00

turbulent buffeting, it can contribute to flow-induced vibrations. The reader is referred to the review paper by Païdoussis (1982).

Early flow-visualization studies (Wallis 1939) described alternate shedding of "eddies" in both in-line and staggered tube banks. More recently, Weaver & Abd-Rabbo (1985) published the results of visualization work on an in-line square bank with pitch-to-diameter ratio ($s/d = 1{\cdot}5$) while Abd-Rabbo & Weaver (1986) and Price *et al.* (1991) investigated a rotated-square bank ($s/d = 1{\cdot}5$) and Polak & Weaver (1995) published results for an equilateral triangular array ($s/d = 1{\cdot}14 - 2{\cdot}67$). The 16 mm film clip by Weaver & Abd-Rabbo (1984) shows transient phenomena in both stationary and vibrating tube banks. Ziada *et al.* (1989) and Ziada & Oengören (1992) also conducted flow-visualization studies of in-line banks with crosswise and streamwise pitch-to-diameter ratios ($s_y/d \times s_x/d$) of $1{\cdot}6 \times 1{\cdot}35$ and $2{\cdot}25 \times 1{\cdot}75$, respectively.

Transient periodic phenomena are characterized by a Strouhal number, Sh, defined by

$$\mathrm{Sh} = \frac{fd}{u_m}, \tag{1}$$

where d is the cylinder diameter, u_m is the bulk velocity in the minimum cross-section, or interstitial velocity, and f is a characteristic frequency. The Strouhal number is to be considered a function of the flow Reynolds number

$$\mathrm{Re} = \frac{\rho u_m d}{\mu}, \tag{2}$$

where ρ is the fluid density, and μ is fluid viscosity. Some authors base Re and Sh on a superficial velocity $U_m = u_m(s_y - d)/s_y$ in place of equations (1) and (2). Various researchers have published Sh data and correlations of data for tube banks (Chen 1968; Fitz-Hugh 1973; Polak & Weaver 1995; Rae & Wharmby 1987; Weaver *et al.* 1986; Žukauskas *et al.* 1988; Žukauskas & Katinas 1988).

Computational fluid dynamics has been used to provide insight into the transport processes within the passages of heat exchangers and elsewhere. These studies enhance (and to some extent offset) the need for expensive and intrusive experimental test rigs. Many numerical studies have been conducted on vortex shedding in single tubes (Braza *et al.* 1984; Borthwick 1986; Eaton 1987; Gresho *et al.* 1984; Jordan & Fromm 1972; Lecointe & Piquet 1984; Sa & Chang 1991); there have been fewer published on vortex shedding past pairs of cylinders (Chang & Song 1990; Ng *et al.* 1997), past two-row banks (Torikoshi *et al.* 1995), or past larger numbers of cylinders (Johnson *et al.* 1993).

To date, most numerical studies on doubly periodic tube banks are for steady, fully developed flow at low Re laminar, or for steady, high Re turbulent flow (Antonopoulos 1979; LeFeuvre 1973). The results of large-eddy simulations for very high Re turbulent flow in tube banks (Pruitt *et al.* 1990; Stuhmillar *et al.* 1988) have also appeared, but there do not appear to be studies of unsteady, fully developed flow in the laminar regime. This paper investigates the stability of laminar fluid flow for in-line square and rotated-square tube banks with a pitch-to-diameter ratio of 2:1. The main goals of the work were to identify the fundamental excitation mechanisms which induce transient periodic behaviour in tube banks, and to perform and display the results of calculations in terms of qualitative and quantitative aspects of the resulting flow fields.

1.2. Numerical Procedure

The solution procedure used in this study is a finite-volume method which has existed for more than two decades. As most of the concepts described below are well known, the

description of the method has been kept brief. The procedure used is a version of the SIMPLE (Semi-Implicit Method for Pressure-Linked Equations) algorithm [Patankar & Spalding (1972); also see Caretto *et al.* (1972), Patankar (1980) and Spalding (1980)].

It is assumed that the transport of some general conserved property ϕ is given by

$$\frac{\partial(\rho\phi)}{\partial t} + \mathrm{div}(\rho \mathbf{u}\phi) = \mathrm{div}(\Gamma \mathrm{grad}\,\phi) + \mathrm{S}, \tag{3}$$

where $\phi = 1$ (continuity), $\phi = i$ (enthalpy) and $\phi = (u, v)$ (momentum).

The finite domain is tessellated into discrete subdomains or cells by means of a structured grid (Beale 1993a). The nonlinear equation (3) is then approximated by linear algebraic equations with the form

$$a_W(\phi_W - \phi_P) + a_E(\phi_E - \phi_P) + a_S(\phi_S - \phi_P) + a_N(\phi_N - \phi_P) + a_T(\phi_T - \phi_P) + \mathrm{S}_P = 0, \tag{4}$$

where the subscripts W, E, S and N refer respectively to the west, east, south and north neighbours of P, and T refers to the value of ϕ at the previous time-step. The linking a-coefficients are evaluated by means of a hybrid scheme (Spalding 1972) for the convection-diffusion terms, and a fully implicit scheme for the transient term. The source term S_P is linearized as

$$S_P = C(V - \phi_P), \tag{5}$$

where C is a source-term coefficient, and V a source-term value consistent with the other terms in the finite-volume equations.

Velocity resolutes in the local curvilinear directions located at staggered-cell locations (Harlow & Welch 1965) are the independent variables in the momentum equations. These are solved with a guessed pressure field (pressure gradient is treated as a source in the momentum equations). At the end of any given "sweep", the velocity field will not satisfy the equation of continuity if the pressure field is incorrect; pressure and velocity correction factors are then computed, and the process is reiterated until the residual errors are reduced to negligibly small values. Some of the grid cells pass through regions of solid material, within which appropriate terms in the finite-volume equations are cut out (Patankar 1980). The computer code utilized was the general-purpose, research-oriented code PHOENICS (Spalding 1982, 1984).

1.3. Boundary Conditions

Ideally, flow-field calculations would be performed over entire banks of tubes. Heat exchangers, however, contain very large numbers of tubes, and it is not feasible to construct a mesh large enough to cover the entire bank, and at the same time fine enough to capture details of the flow in the boundary layer and wake of every tube; so, it is necessary to differentiate between calculations on the overall mechanical and thermal performance of heat exchangers, and detailed simulations within the passages of the apparatus (Spalding 1981a, b; Beale 1997a, b). For the latter, it is required to develop a rationale based on one or more typical modules, on the assumption that unsteady, fully developed, periodic conditions prevail. The general approach taken is to consider at least two complete modules in the streamwise x-direction, apply a transient-periodic disturbance at the upstream module, measure the downstream response, then feed this back as the disturbance later, after at least one cycle of motion (and preferably several) have elapsed. Figure 1 shows the modules considered here.

In conventional flow problems, the inlet and outlet are defined unambiguously. Many boundary prescriptions are possible, though typically a constant inlet mass flux

$S_P = \dot{m} = \rho A u$ is specified in the continuity equation together with upstream scalar sources $S_P = \dot{m}\phi = \rho A u \phi$. The value of the pressure must also be fixed somewhere in the flow field, and this may be achieved by a linear relationship between the downstream in-cell pressure p_P and some external value p_∞ (often taken to be zero), by setting a mass source $S_P = C(p_P - p_\infty)$ in the continuity equation. The conservative form of the SIMPLE algorithm ensures a balance between the inlet and exit mass sources or sinks, while the magnitude of C controls how close the p_p and p_∞ will be.

It is assumed that a transient-periodic behaviour has been established in the interior of the tube bank, either spontaneously or by some externally applied upstream stimulus. For steady, fully developed flow (Beale & Spalding 1998), the velocity field is considered to be doubly periodic, with $\mathbf{u}(x, y) = \mathbf{u}(x + s_x, y) = \mathbf{u}(x, y + s_y)$ and the pressure p at any position may be considered to be composed of a linear term in the streamwise x-direction and a doubly periodic term. For fully developed transient flow, there will be temporal fluctuations in the velocity field, so that

$$\mathbf{u}(x, y, t) = \mathbf{u}(x, y + s_y, t + \tau_y) = \mathbf{u}(x + s_x, y, t + \tau_x) \tag{6}$$

and,

$$p(x, y, t) = p(x, y + s_y, t + \tau_y) = p(x + s_x, y, t + \tau_x) + \Delta\bar{p}_{\text{row}}, \tag{7}$$

where the average row pressure drop $\Delta\bar{p}_{\text{row}}$ is just

$$\Delta\bar{p}_{\text{row}} = \frac{1}{t}\int_t p(x, t) - p(x + s_x, t)\,\mathrm{d}t, \tag{8}$$

$$p(x, t) = \frac{\displaystyle\int_{y=-s_y/2}^{s_y/2} p(x, y, t)\,\mathrm{d}y}{\displaystyle\int_{y=-s_y/2}^{s_y/2} \mathrm{d}y} \tag{9}$$

evaluated within the fluid phase only, and τ_x and τ_y are phase differences between the fluctuating components at x and $x + s_x$, and at y and $y + s_y$, respectively. An immediate problem arises, namely that τ_x and τ_y are not known *a priori*. In the absence of any further information, cyclic boundary conditions were imposed along the length of the lateral boundary (*a*-*b*-*c* and *a*′-*b*′-*c*′). Nontrivial values of τ_x were, however, allowed to evolve, as described further below.

Initial fields for state variables were obtained from a partially converged solution to the steady-flow problem in preference to the fully converged solution, since the latter had the tendency to elongate and dissipate the initial wake vortices at the outset of the calculations.

The methodology adopted was the following (see Figure 1).

(i) An upstream disturbance $V_0 \sin(2\pi f_0 t)$ was applied to the v-momentum equation between cylinders A and B [Figure 1(a)] for an initial period of three complete cycles. A uniform flow in the x-direction, $|\mathbf{u}| = u_m$, was prescribed at the inlet *a*-*a*′.

(ii) At each time-step, the downstream lateral v-responses between cylinders B and C, and the **u**-values along *b*-*b*′ were measured and stored in ring buffers.

(iii) After the initial period, the stored **u**-values were applied upstream as the inflow along *a*-*a*′, and the v-responses as the upstream disturbances between A and B.

Steps (ii) and (iii) were then reiterated until either the disturbance died out, or a fully developed transient periodic behaviour was obtained. Treatment of the in-line and staggered geometries was essentially identical, apart from the presence of additional rows of

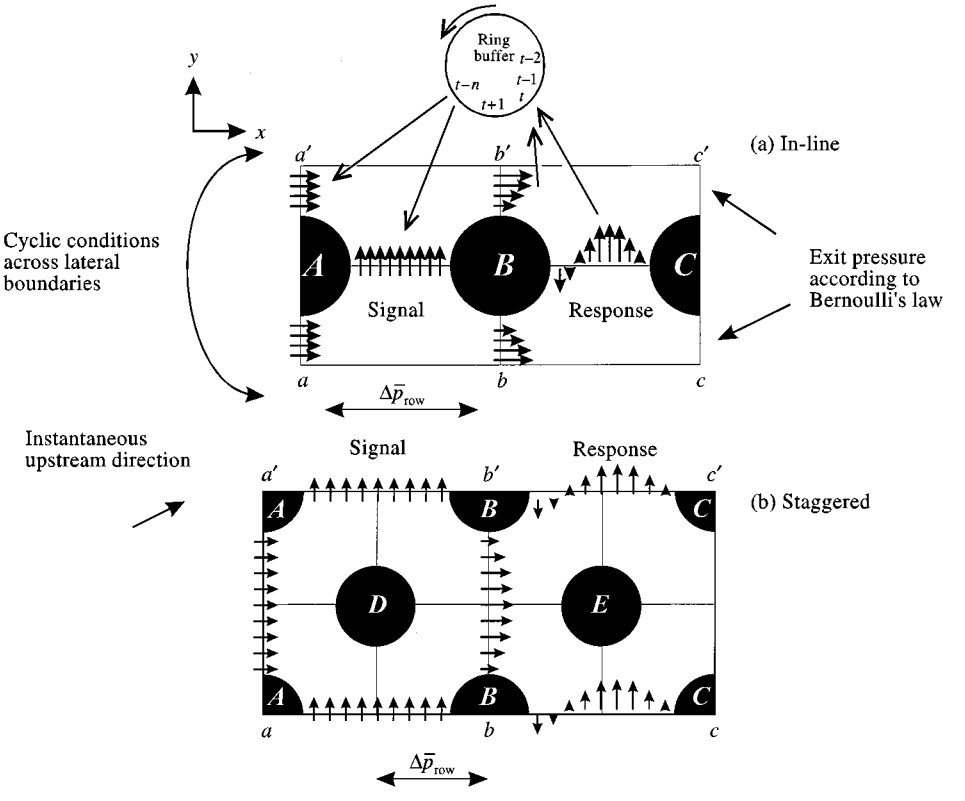

Figure 1. Boundary condition prescription for in-line and staggered tube banks.

tubes in the latter case, as indicated in Figure 1(b). Because the domain boundaries were chosen to correspond to inlet-exit zones, upwind boundary values were presumed to predominate, and streamwise diffusion was neglected (though, in fact, both inflow and outflow may occur for a brief moment at all boundaries for the staggered geometry). In certain cases, the lateral feedback mechanism was disabled in order to generate spontaneously induced periodic flow. The streamwise inlet boundary conditions, however, were always prescribed as described above. The downstream pressure p_p was computed from the downstream velocity field by means of Bernoulli's law with $p_p = -\frac{1}{2}\rho u_p^2$, where p_P and u_P are in-cell values of velocity and pressure near the exit. This is achieved with a coefficient $C = \sqrt{2\rho/p_P}$ and a value $V = 0$ along the outlet cell row in the continuity (pressure correction) equation.

Heat transfer was also modelled as part of this study, and was assumed to occur under conditions of constant wall-heat flux. The temperature field, far from the entrance to the tube bank, is considered to be such that

$$T(x, y, t) = T(x, y + s_y, t + \tau_y) = T(x + s_x, \mathrm{y}, t + \tau_x) + \Delta\bar{T}_b, \tag{10}$$

and $\Delta\bar{T}_b$ is the difference in time-average bulk fluid temperature between two adjacent rows

$$\Delta\bar{T}_b = \frac{1}{t}\int_t (T_b(x, t) - T_b(x + s_x, t))\,\mathrm{d}t, \tag{11}$$

where

$$T_b = \frac{\int_{y=-s_y/2}^{s_y/2} \rho u(x, y, t) T(x, y, t)\, \mathrm{d}y}{\int_{y=-s_y/2}^{s_y/2} \rho u(x, y, t)\, \mathrm{d}y} \tag{12}$$

is evaluated in the fluid alone. The time-average upstream bulk temperature was set to be zero by subtracting the time-average value $\rho c_p \bar{T}_b$ across b-b' from previously stored enthalpy values prior to back-substitution at a-a'.

1.4. Parameters Considered

A number of tests were conducted to investigate the stability of the flow to induced perturbations, capture features of the transient nature of fluid flow, and the excitation mechanism in the passages of tube banks. Calculations were performed to investigate:

(i) the stimulated induction of a transient periodic behaviour and the passive generation of a transient oscillation in the absence of any specific excitation mechanism;

(ii) the threshold Re above which instabilities arise and the influence of the excitation frequency f_0 of the initial applied disturbance on the long-term frequency of the response f;

(iii) the influence of the amplitude V_0 (this included the case $V_0 = 0$) on the final amplitude V and frequency f of the simulation;

(iv) calculated values of Sh as compared to data obtained from experimental data and empirical correlations; and

(v) the effect of the vortex generation process on the pressure applied to the cylinder walls, as well as on quantitative performance measures such as lift, drag and heat-transfer coefficients.

2. RESULTS

The results were obtained with a total of 640 time-steps (staggered) or 960 time-steps (in-line) which corresponds to eight cycles per run, on the assumption that $\mathrm{Sh}_0 = f_0 d/u_m$ of 0·2 (staggered) or 0·1 (in-line), at 40 sweeps per time-step, and 20 iterations per sweep. Animated sequences of velocity vectors, particle traces, streamlines, pressure and temperature contours were prepared by means of flow visualization software (Watson *et al.* 1990). Figure 2 shows the stimulated response to an upstream spanwise disturbance for the staggered tube bank. The lateral v-velocities at monitor points located midway between cylinders A and B (upstream) and between B and C (downstream) are presented. It can be seen that, whereas at Re = 30 the response dies down with time, at Re = 300 the signal is amplified downstream and a stable periodic behaviour results.

2.1. Flow Visualization Studies

Figure 3 shows a sequence of six plots of velocity vectors, and illustrates the time-dependent flow patterns in the central zone [Figure 1(b), b-b'] over one complete cycle at Re = 300 for the rotated square tube bank. Figure 4 shows streamlines, Figure 5 pressure contours, and Figure 6 temperature contours over the same sequence. Figures 7–10 show similar plots of velocity vectors, streamlines and temperature contours for the upstream module of the in-line bank [Figure 1(a)] at Re = 300.

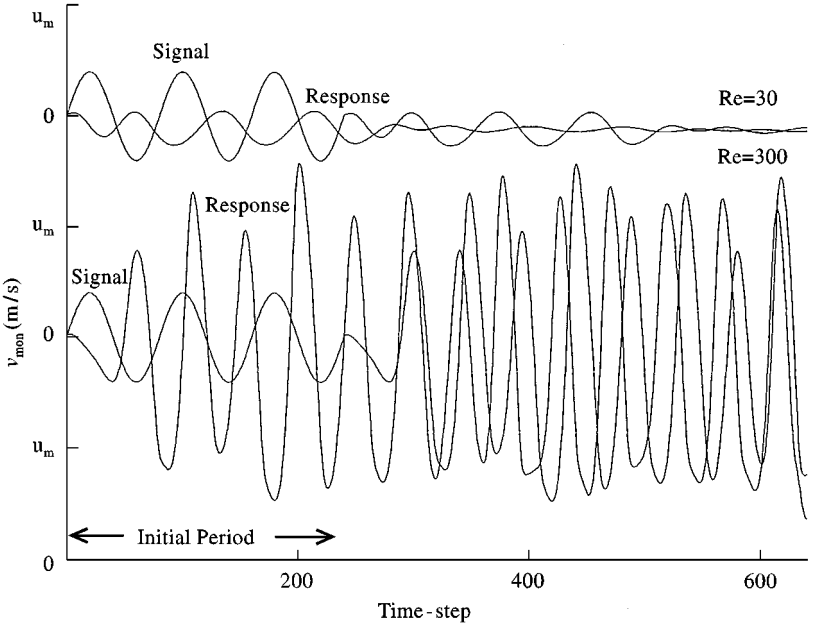

Figure 2. Response to feedback mechanism.

2.2. Monitor Point And Convergence Data

Figure 11 shows values of the crosswise v-velocity at a monitor point located midway between cylinders A and B [Figure 1(b)] as a function of time at various Re values for the rotated square bank. Figure 12 is a similar plot at various applied frequencies, while Figure 13 shows the influence of the amplitude of the applied disturbance: the motion is independent of the magnitude and frequency of the applied disturbance. Figure 14 shows the influence of the applied frequency on the transient motion for the in-line bank. Traces of monitor point, crosswise velocity are displayed together with the initial applied disturbance for Sh_0 of 0·05, 0·1, 0·2 and 0·5. The monitor point is located halfway between cylinders B and C in Figure 1(a). Table 1 shows values of Sh for both in-line and staggered geomeries as the number of time-steps and sweeps is increased.

2.3. Drag And Heat Transfer

Tables 2 and 3 are summaries of results for stimulated and spontaneous behaviour, respectively, within the rotated square tube bank; Table 4 gives data for the in-line geometry. All values are averaged over the last half of each simulation. The final frequency f is calculated from the v-velocity at the monitor point. The quantity $f\tau_x$ is the fraction of a cycle by which the upstream transient leads the value at the subsequent row; this is computed from the v-values at two monitor points. The Euler number Eu is defined as the normalized mean pressure difference between two rows:

$$\mathrm{Eu} = \frac{\Delta \bar{p}_{\mathrm{row}}}{\frac{1}{2}\rho u_m^2}. \tag{13}$$

Both the time-average value μ and the sample standard deviation σ are given in Tables 2–4. Lift and drag coefficients c_L and c_D are defined as the net forces due to lift and drag per

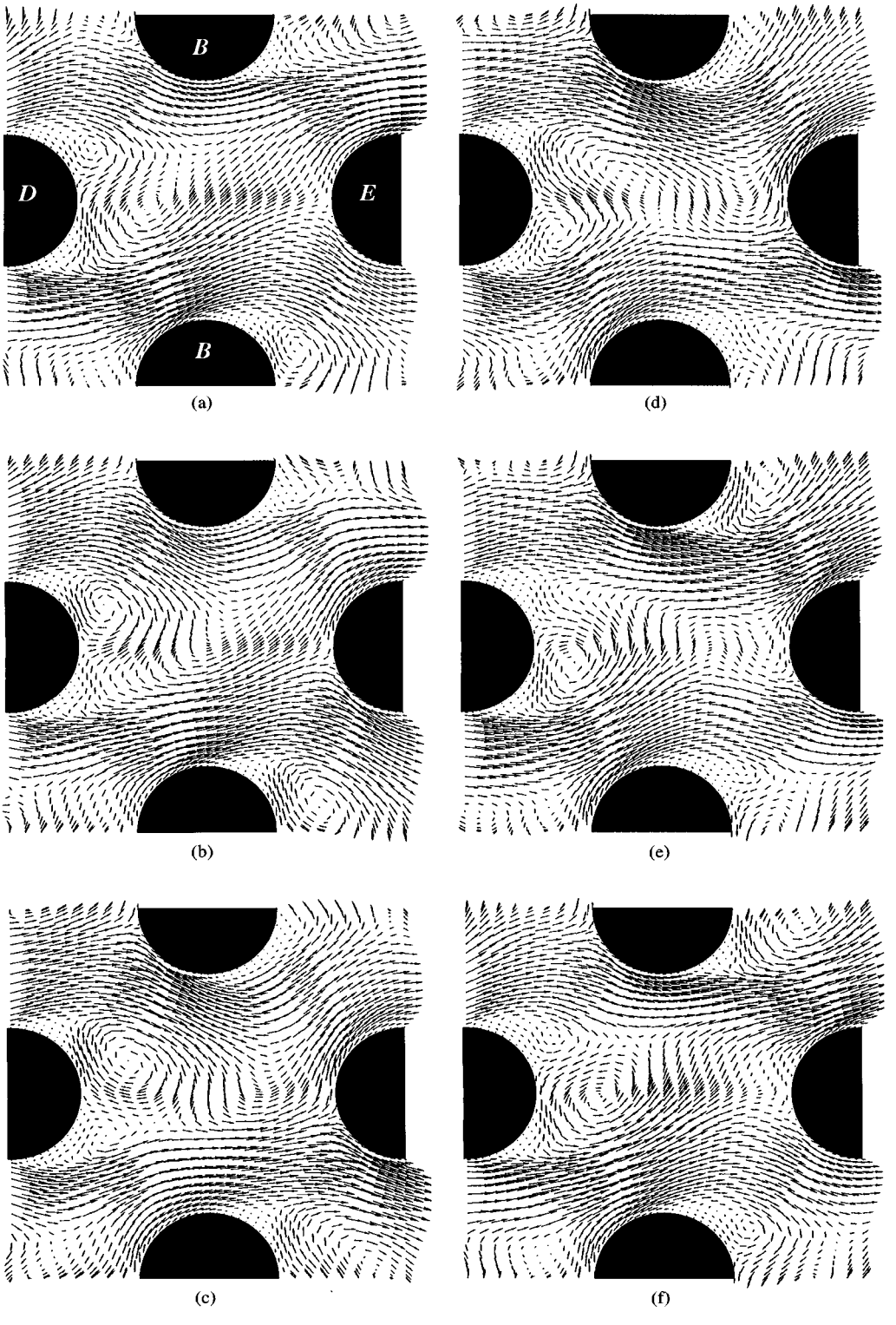

Figure 3. Velocity vectors for Re = 300; staggered bank.

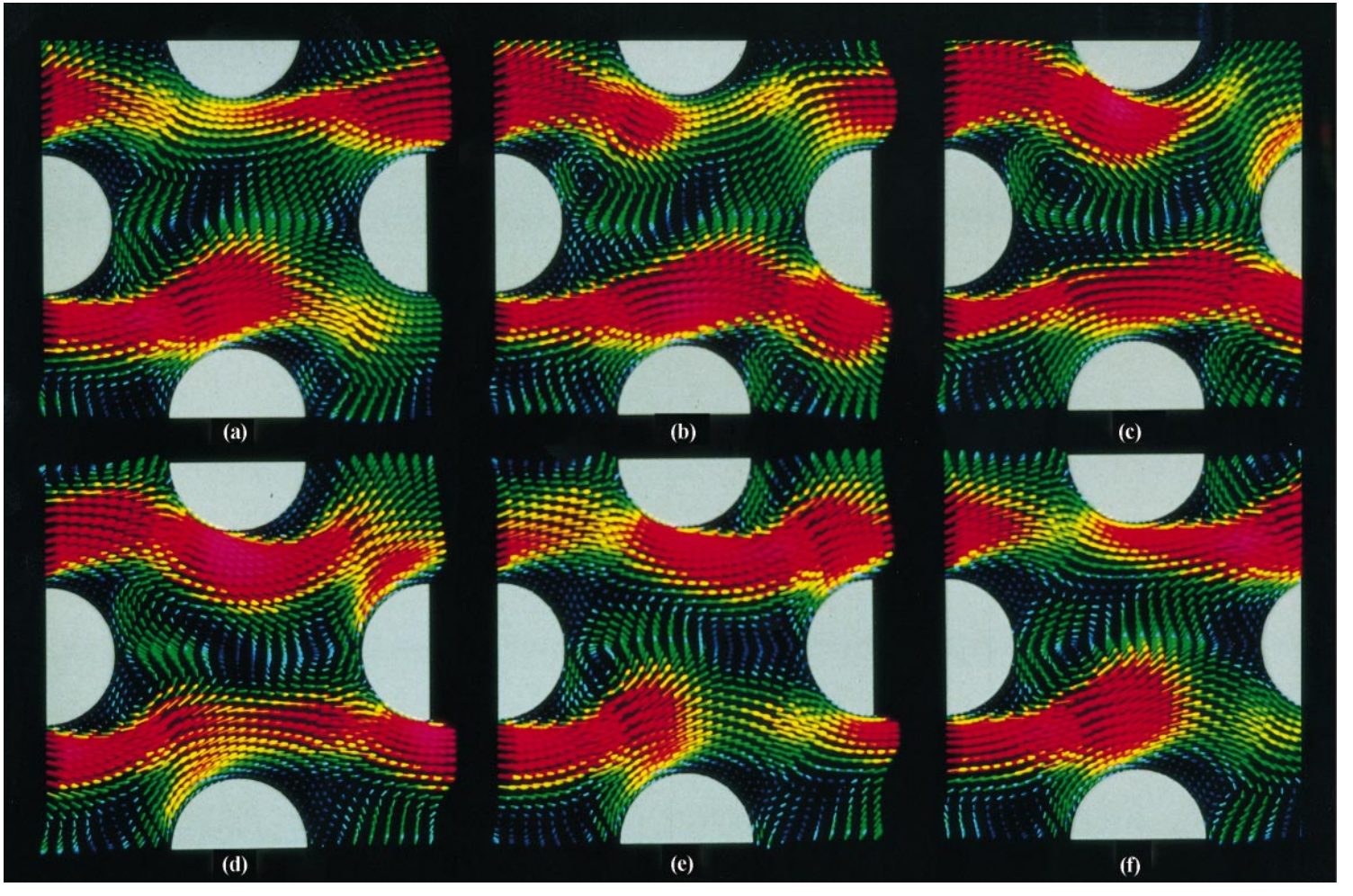

Plate 1. Colour reduction of the results of Figure 3.

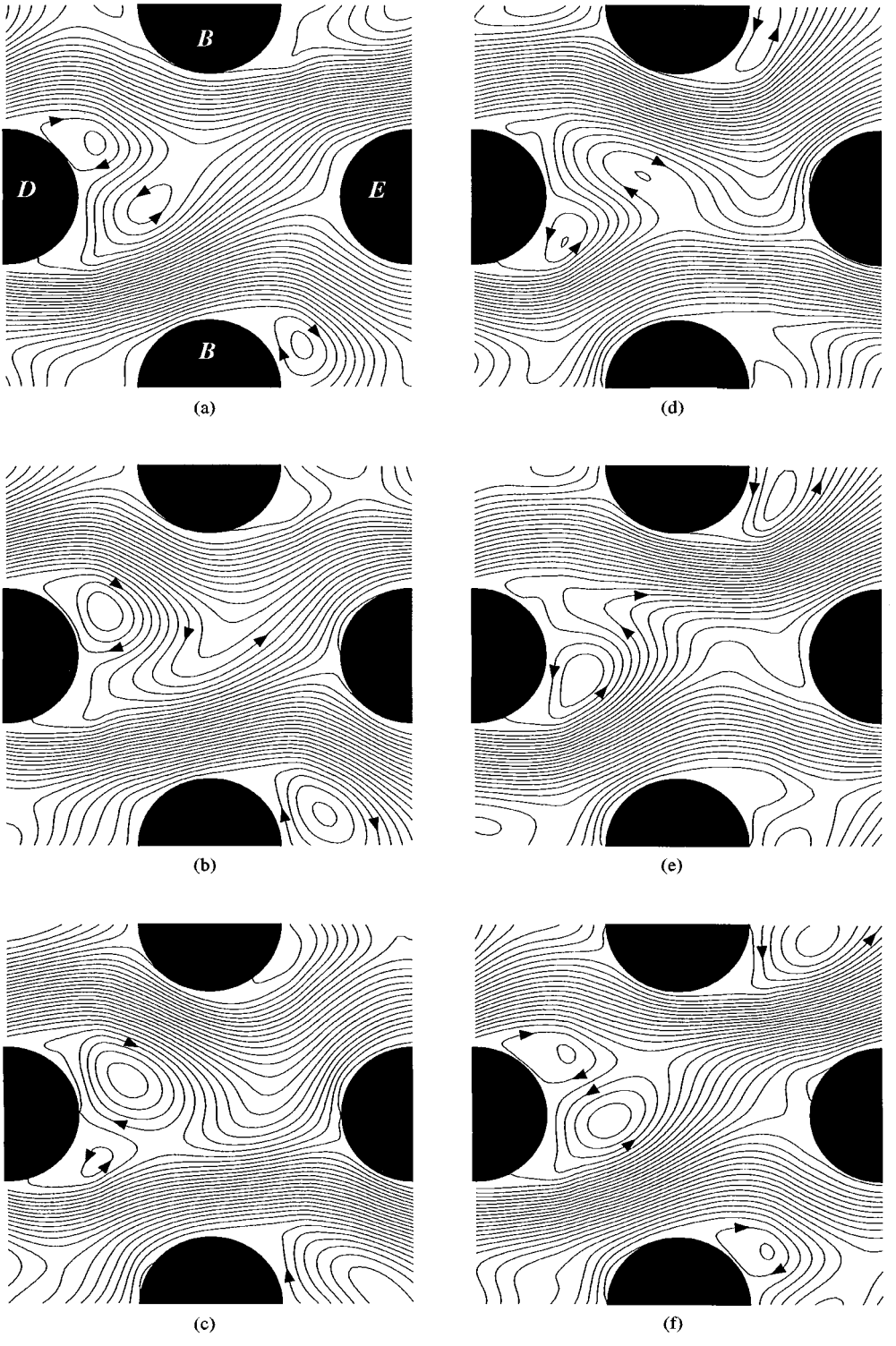

Figure 4. Streamlines for Re = 300; staggered bank.

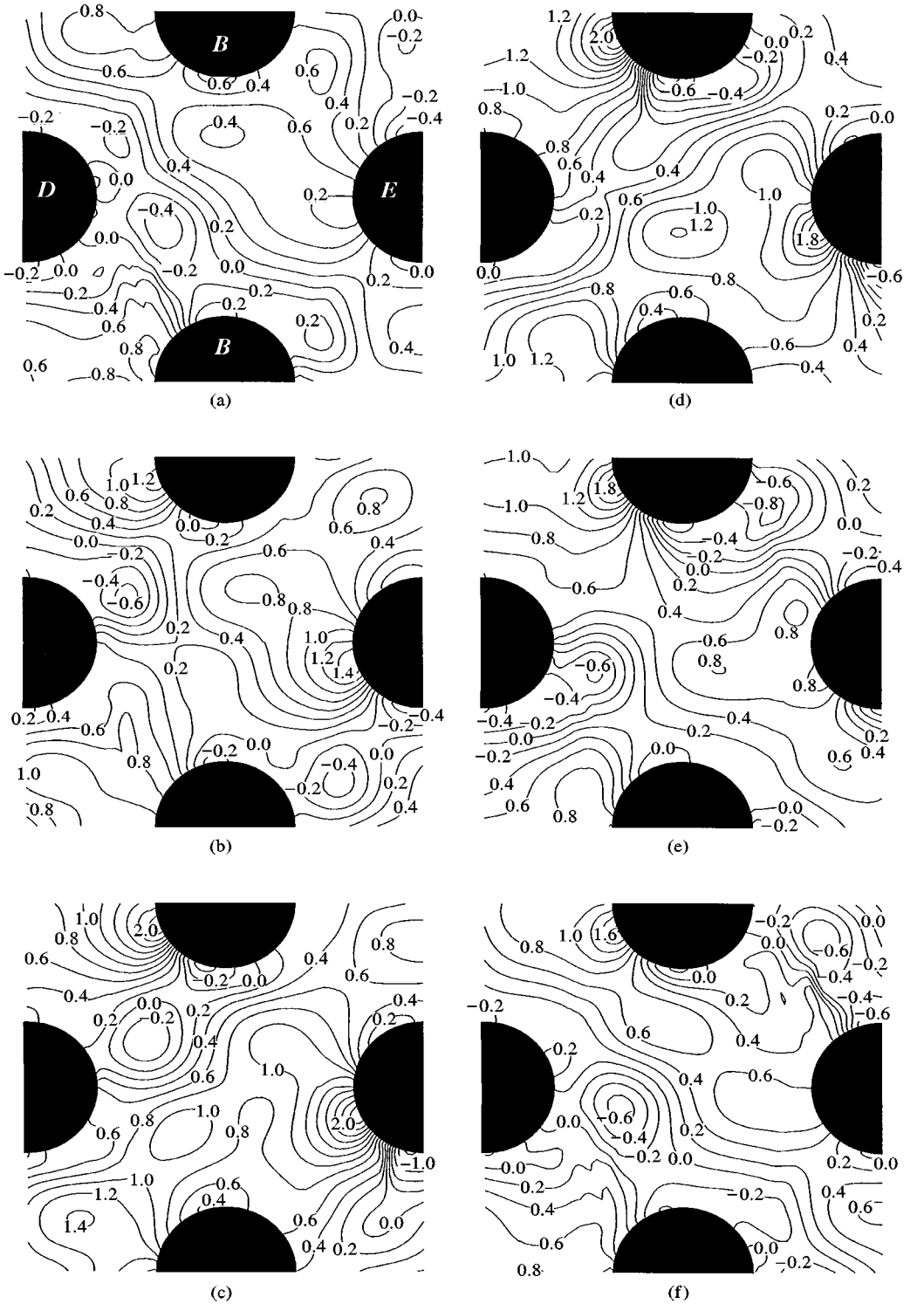

Figure 5. Pressure contours for Re = 300; staggered bank.

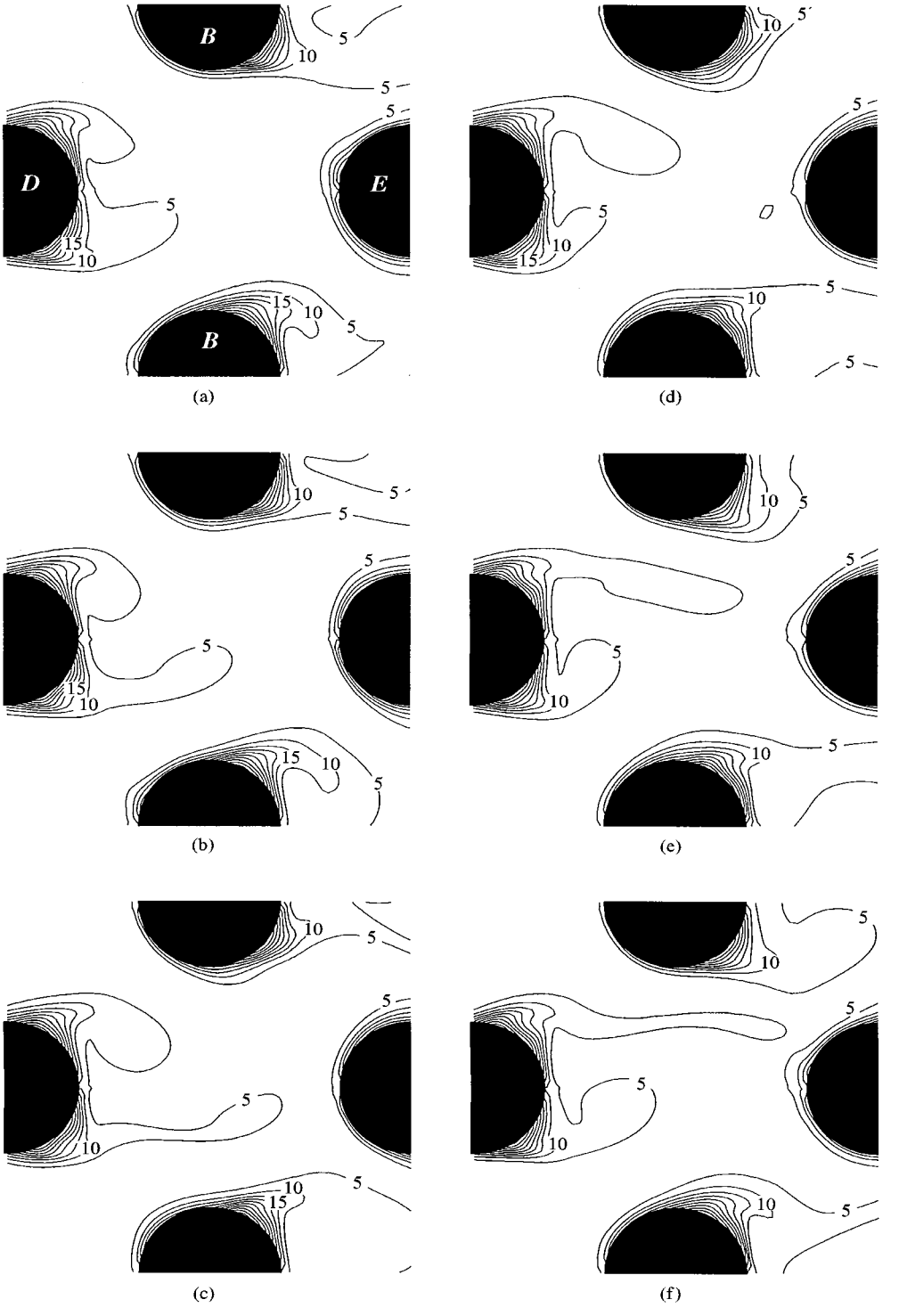

Figure 6. Temperature contours (°C) for Re = 300; staggered bank.

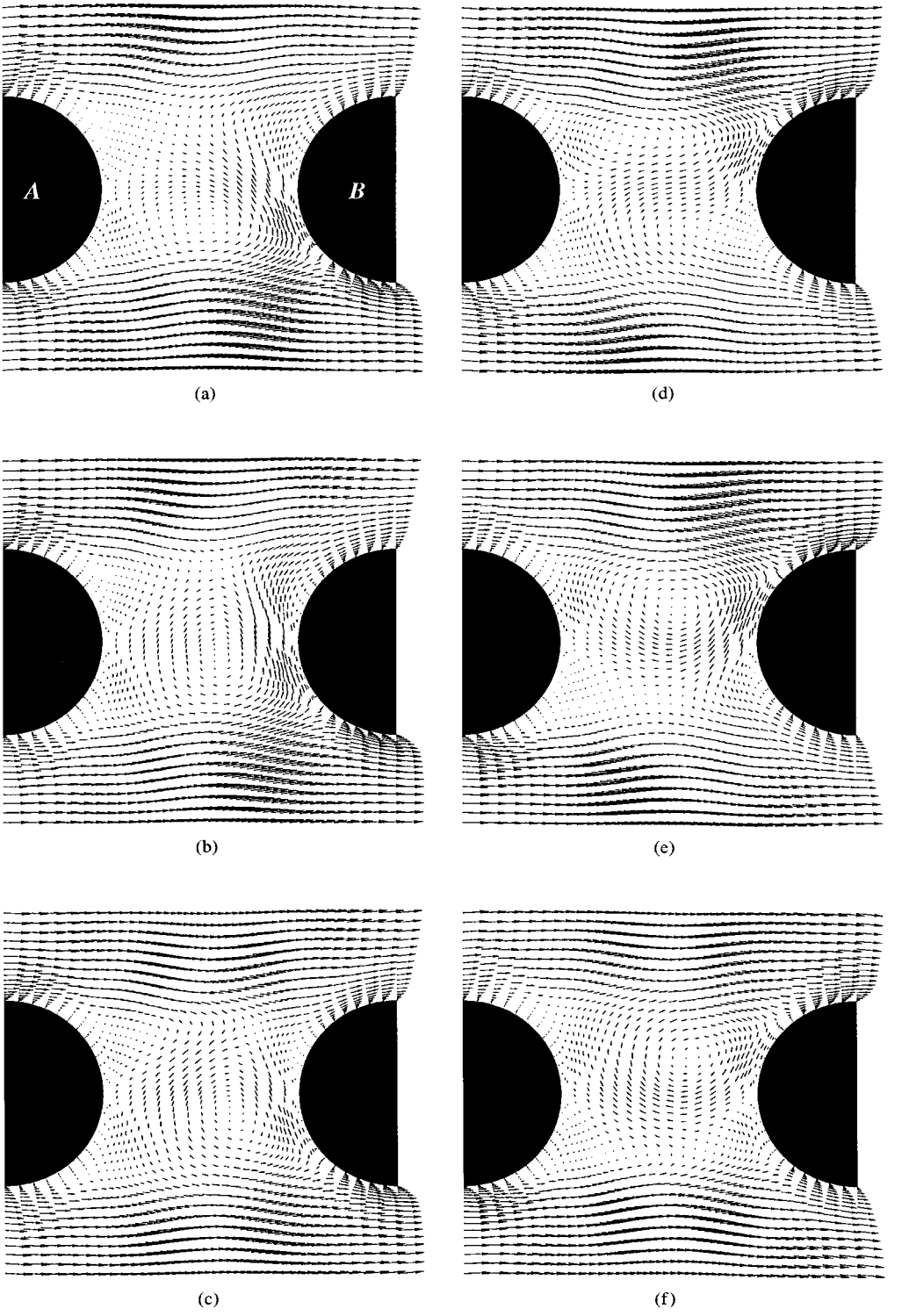

Figure 7. Velocity vectors for Re = 300; in-line bank.

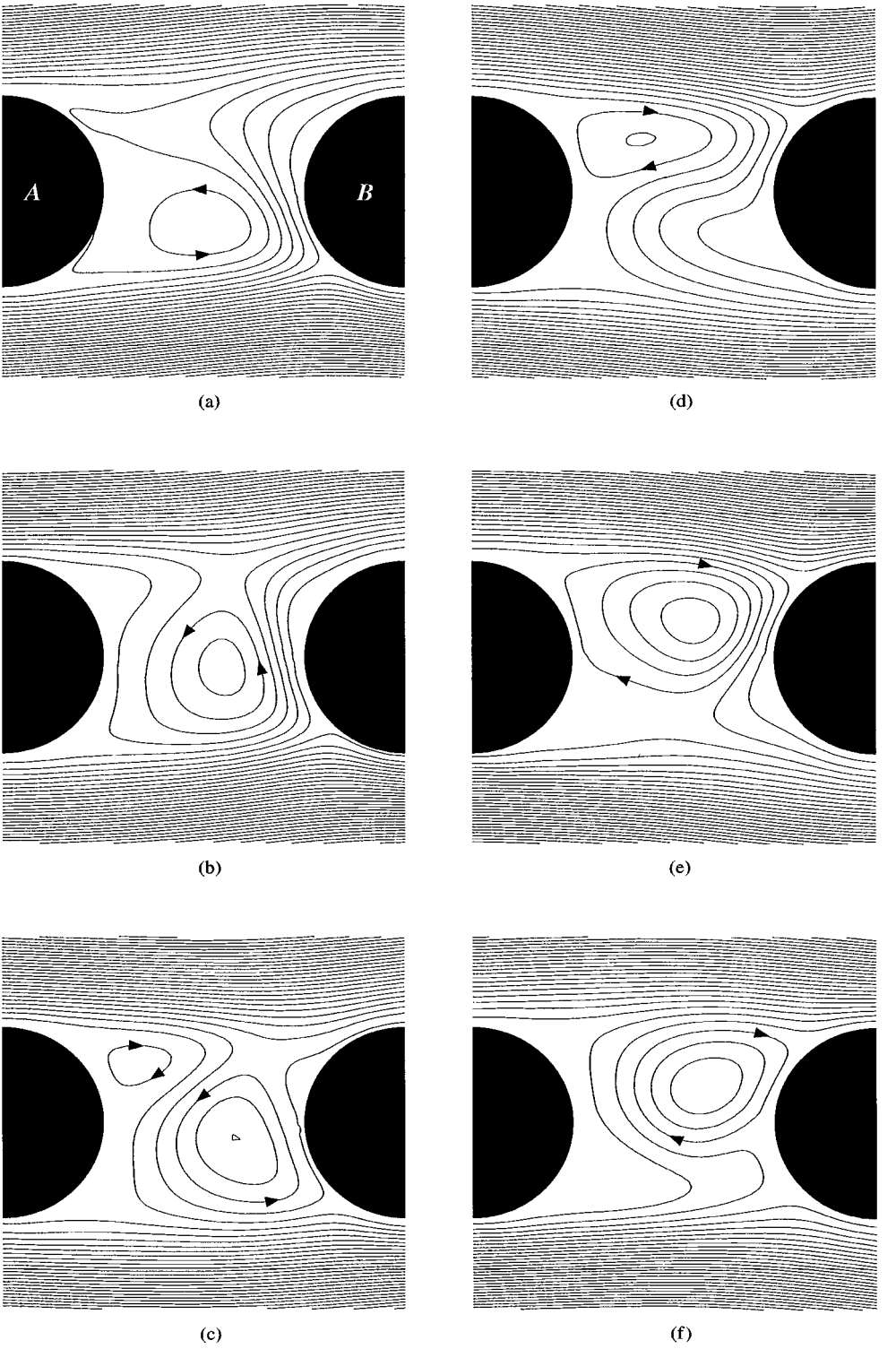

Figure 8. Streamlines for Re = 300; in-line bank.

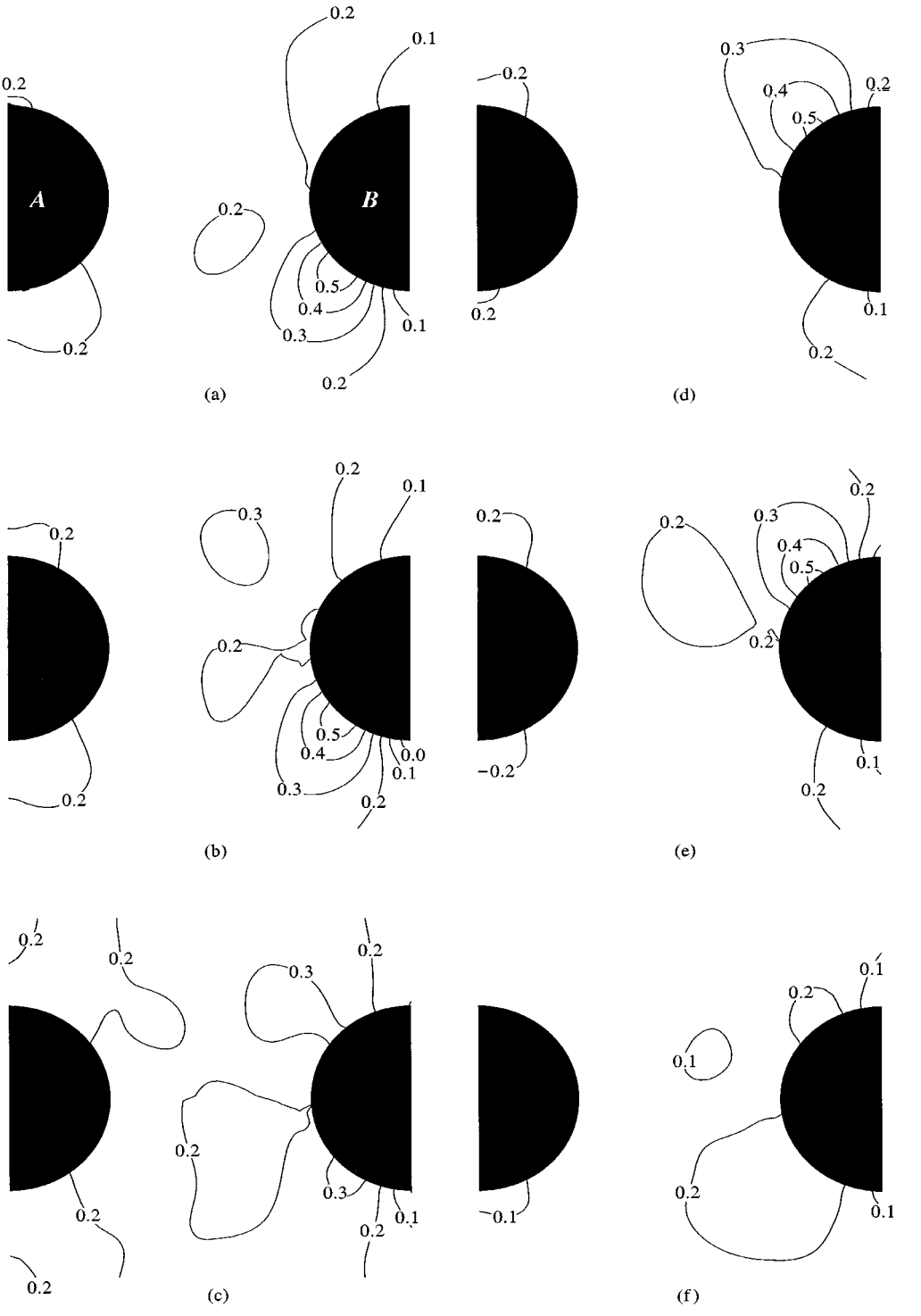

Figure 9. Pressure contours for Re = 300; in-line bank.

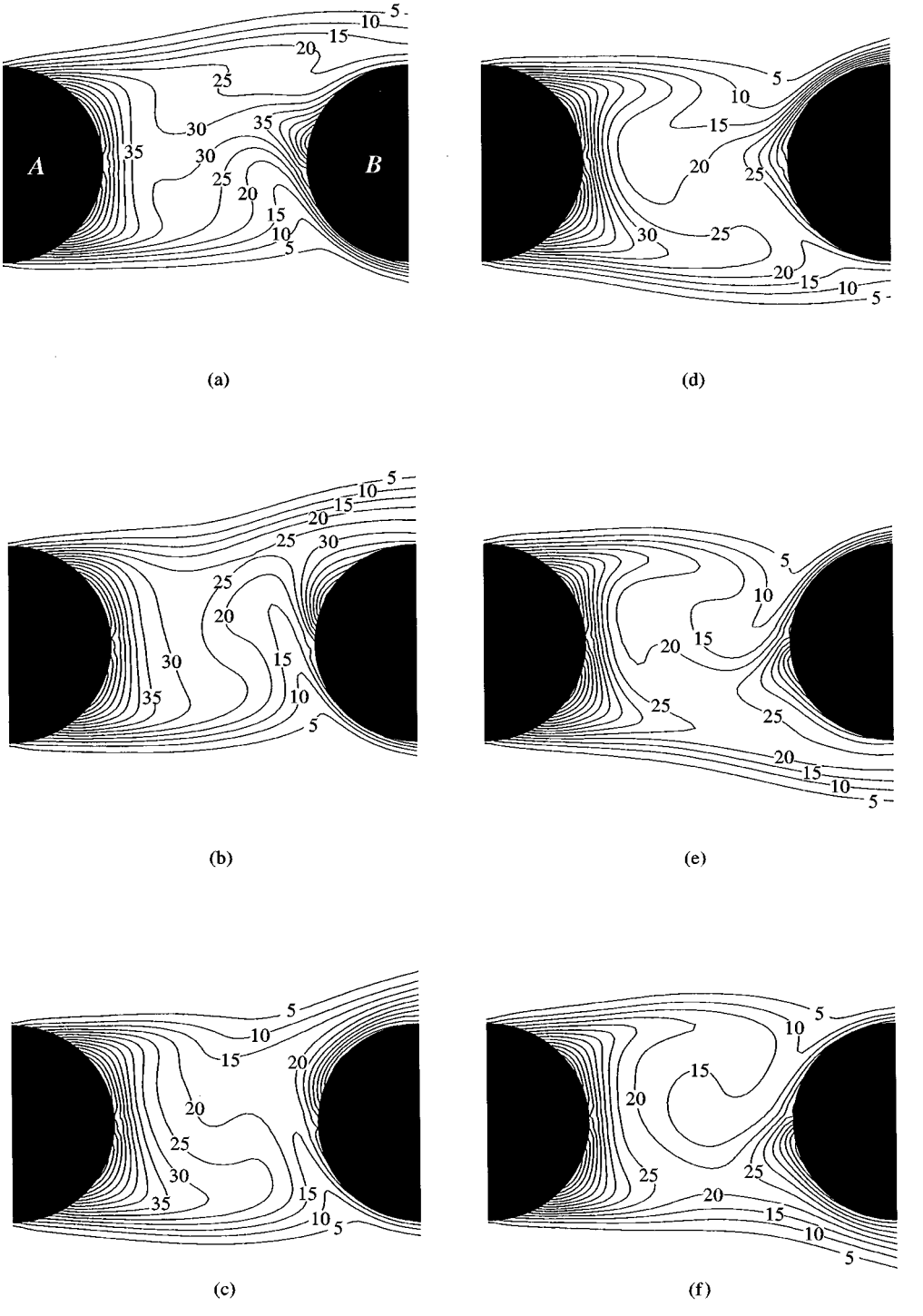

Figure 10. Temperature contours (°C) for Re = 300; in-line bank.

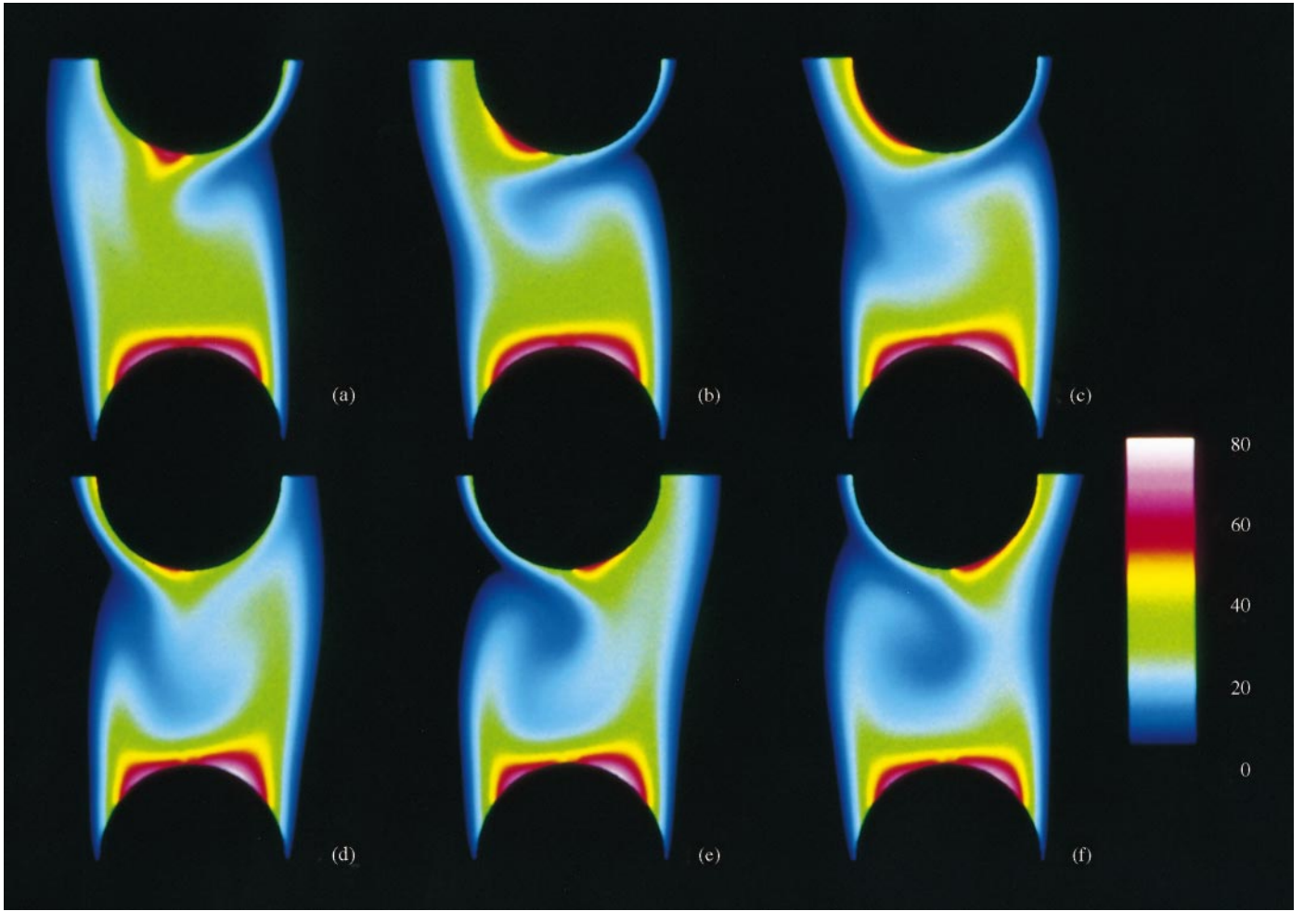

Plate 2. Colour rendition of the results of Figure 10.

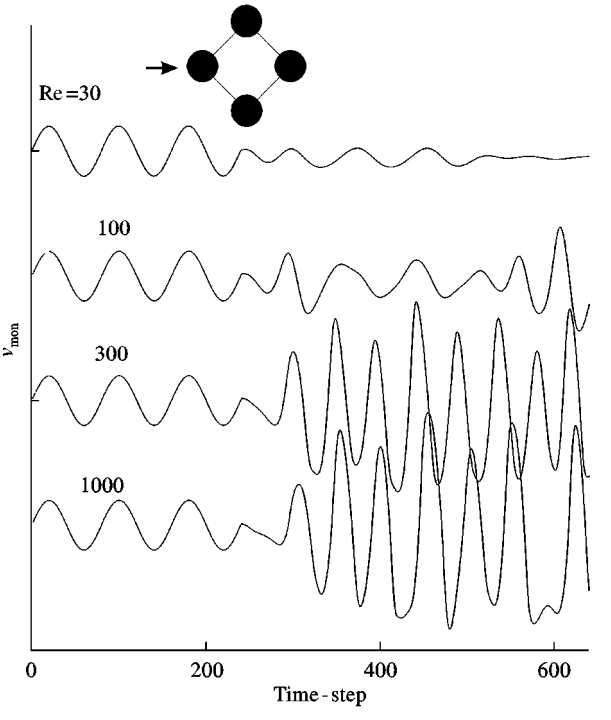

Figure 11. Effect of Re for $Sh_0 = 0{\cdot}2$; staggered bank.

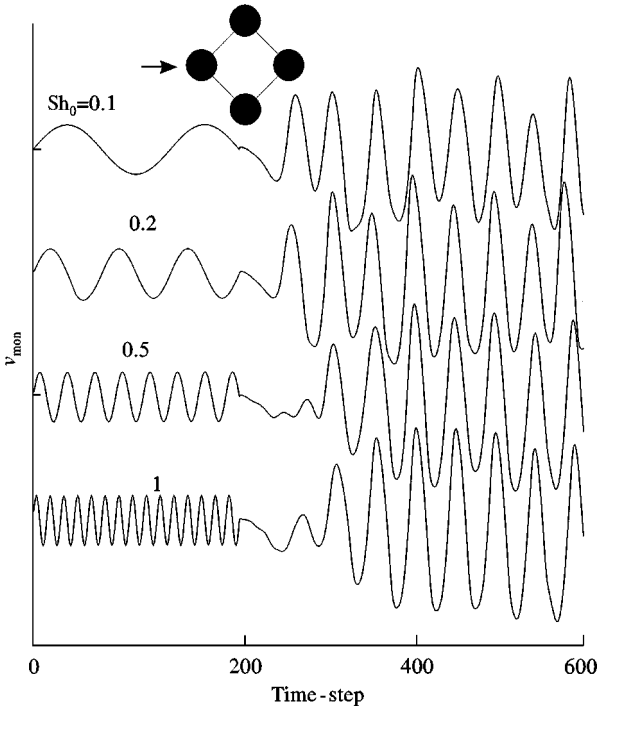

Figure 12. Effect of f_0 for Re = 300; staggered bank.

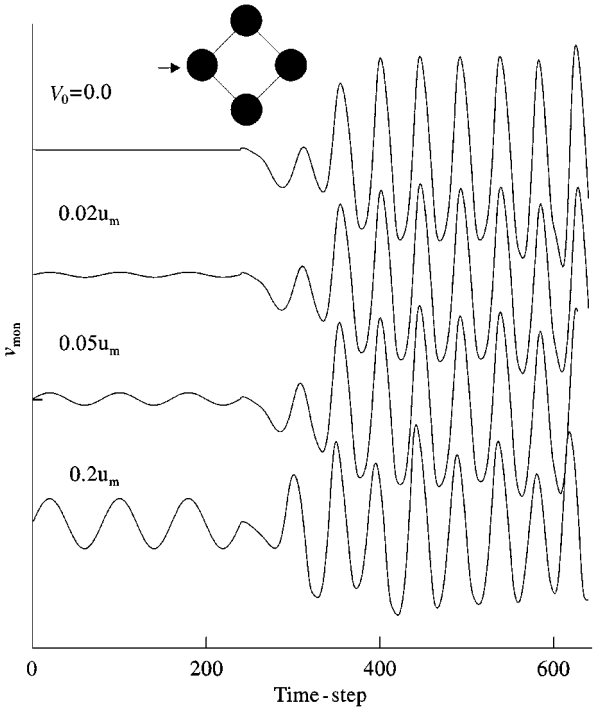

Figure 13. Effect of V_0 for Re = 300, Sh_0 = 0·2; staggered bank.

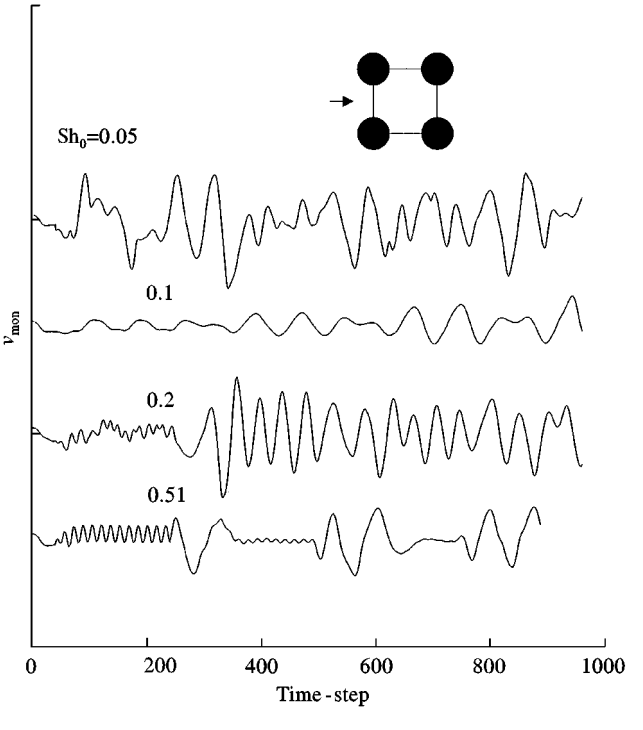

Figure 14. Effect of f_0 for Re = 300; in-line bank.

TABLE 1

Solution independence studies, Re = 300

Type	Sweeps	Time-steps	Sh
In-line square	40	480	0·0891
In-line square	40	960	0·0920
In-line square	100	960	0·0925
In-line square	100	1960	0·0933
Rotated square	40	320	0·289
Rotated square	40	640	0·353
Rotated square	100	640	0·358
Rotated square	100	1280	0·356

TABLE 2

Staggered geometry, stimulated response, $Sh_0 = 0{\cdot}2$, $V_0 = 0{\cdot}2u_m$

Re	Sh	$f\tau_x$	Eu		c_D		c_l	Nu	
	(μ)	(μ)	(μ)	(σ)	(μ)	(σ)	(σ)	(μ)	(σ)
30	—	—	0·92	0·06	2·88	0·05	0·017	6·4	0·1
100	0·27	0·73	0·57	0·06	1·88	0·17	0·047	8·9	0·3
300	0·35	0·89	0·37	0·18	1·73	0·31	0·062	15·5	1·1
1000	0·31	0·76	0·25	0·19	1·61	0·32	0·050	30·0	1·9
3000	0·26	0·82	0·16	0·20	1·32	0·33	0·027	56·6	2·9

TABLE 3

Staggered geometry, spontaneous response, no lateral feedback, $V_0 = 0$

Re	Sh	$f\tau_x$	Eu		c_D		c_l	Nu	
	(μ)	(μ)	(μ)	(σ)	(μ)	(σ)	(σ)	(μ)	(σ)
30	—	—	0·93	0·00	2·87	0·00	0·001	6·3	0·0
100	0·22	—	0·61	0·02	1·92	0·06	0·007	9·1	0·3
300	0·35	0·95	0·25	0·22	1·69	0·47	0·061	15·5	1·0
1000	0·30	0·75	0·02	0·24	1·51	0·45	0·056	29·6	2·4
3000	0·31	0·75	0·02	0·25	1·34	0·42	0·033	54·9	3·7

TABLE 4

In-line geometry, stimulated response, $Sh_0 = 0{\cdot}1$, $V_0 = 0{\cdot}2u_m$

Re	Sh	$f\tau_x$	Eu		c_D		c_l	Nu	
	(μ)	(μ)	(μ)	(σ)	(μ)	(σ)	(σ)	(μ)	(σ)
100	0·09	0·44	0·317	0·018	1·313	0·046	0·066	3·92	0·069
300	0·09	0·41	0·171	0·055	0·747	0·122	0·051	6·73	0·47
1000	0·12	0·55	0·104	0·130	0·630	0·214	0·077	17·4	2·2
3000	0·10	0·52	0·193	0·404	1·048	0·553	0·044	40·8	3·9

projected area, normalized with respect to $\frac{1}{2}\rho u_m^2$ and computed as follows:

$$c_D = \frac{1}{t}\int_t \frac{1}{\rho u_m^2}\left(\int_0^{\pi}(p\cos\theta + \tau_w \sin\theta)\,\mathrm{d}\theta + \int_{\pi}^{2\pi}(p\cos\theta - \tau_w \sin\theta)\,\mathrm{d}\theta\right)\mathrm{d}t, \tag{14}$$

and

$$c_L = \frac{1}{t}\int_t \frac{1}{\rho u_m^2}\left(\int_0^{\pi}(-p\sin\theta + \tau_w \cos\theta)\,\mathrm{d}\theta - \int_{\pi}^{2\pi}(p\sin\theta + \tau_w \cos\theta)\,\mathrm{d}\theta\right)\mathrm{d}t, \tag{15}$$

where θ is the angle from the front of the cylinder. The average Nusselt number $\overline{\mathrm{Nu}}$ is defined by

$$\overline{\mathrm{Nu}} = \frac{\bar{h}d}{k}, \tag{16}$$

where

$$\bar{h} = \frac{2\pi\dot{q}_w}{\int_0^{2\pi}(T_w - \bar{T}_b)\,\mathrm{d}\theta}, \tag{17}$$

and $\dot{q}_w$ is the constant wall-heat flux, T_w the wall temperature and $\bar{T}_b$ the time-average bulk temperature in the upstream inter-tube space for the tube under consideration.

Figures 15 and 16 show the instantaneous pressure coefficient c_p for both in-line-square and rotated-square geometries, as a function of the angle, θ, from the front edge of the

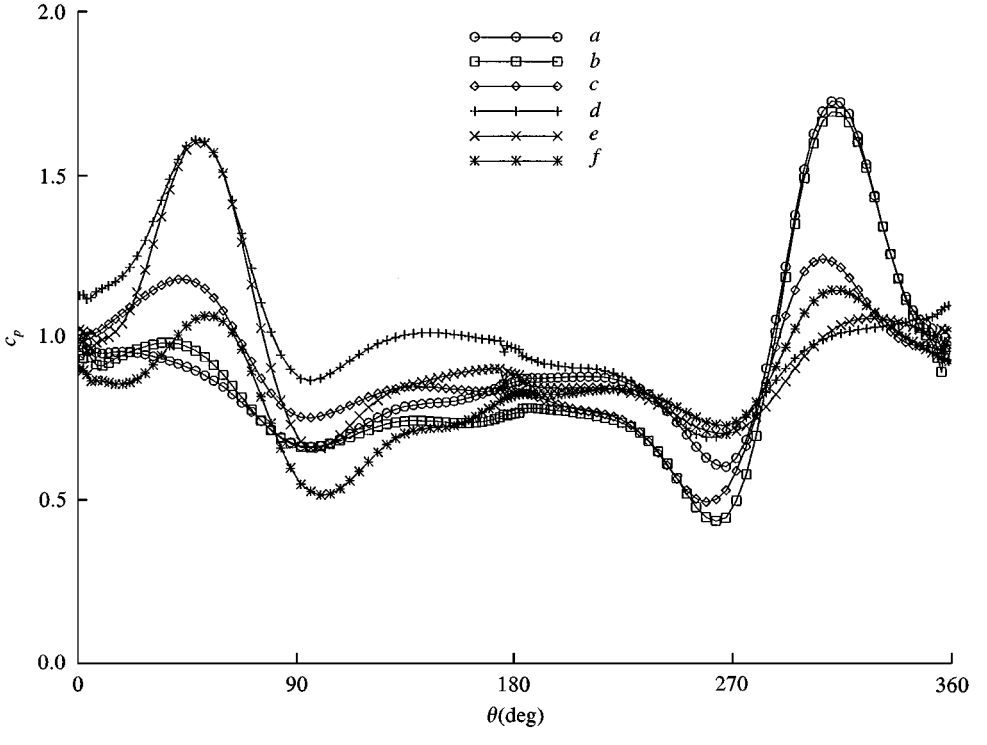

Figure 15. c_p versus θ for Re = 300, $\mathrm{Sh}_0 = 0{\cdot}2$, $V_0 = 0{\cdot}2u_m$; in-line bank.

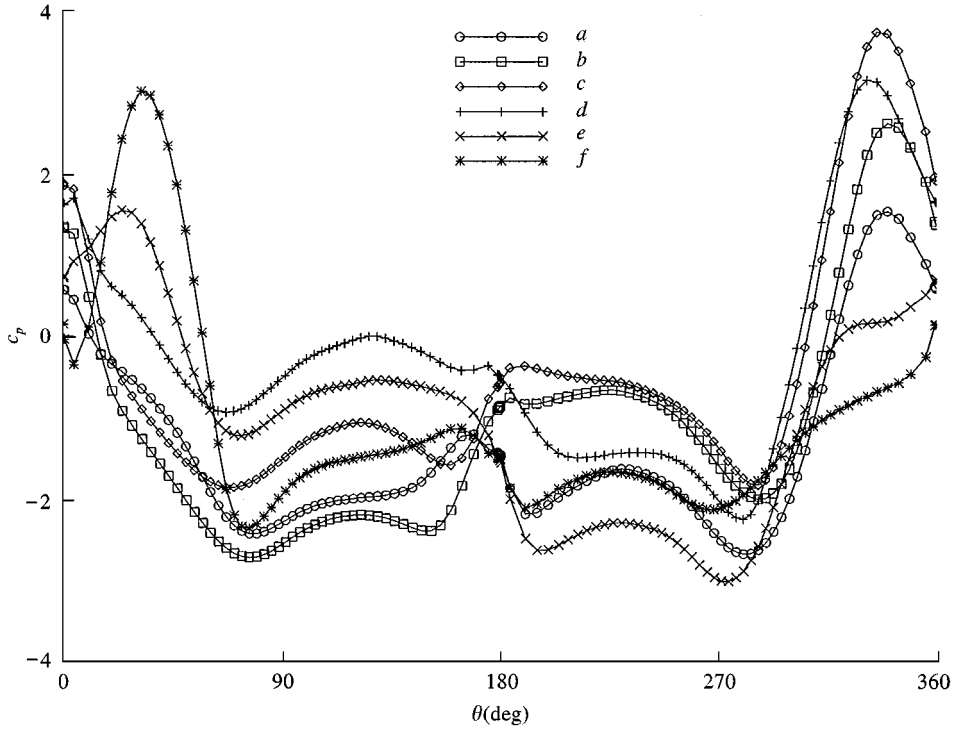

Figure 16. c_p versus θ, for Re = 300, $Sh_0 = 0{\cdot}1$, $V_0 = 0{\cdot}2u_m$; staggered bank.

cylinder. The local-pressure coefficient is defined as

$$c_P = 1 - \frac{\bar{p}(0) - p(\theta)}{\frac{1}{2}\rho u_m^2}, \tag{18}$$

where $\bar{p}(0)$ is the time-average pressure at $\theta = 0^\circ$. The curves a–f in Figures 15 and 16 correspond to the data shown for the eight captions in Figures 3–10. Figure 17 shows the friction coefficient c_f against θ defined as

$$c_f = \pm \frac{\tau_w}{\frac{1}{2}\rho u_m^2}, \tag{19}$$

where the shear stress is computed from the velocity gradient at the wall $\tau_w = \mu \partial u/\partial n$, and the sign of c_f is taken to be positive for $0^\circ \leq \theta \leq 180^\circ$ and negative for $180^\circ \leq \theta \leq 360^\circ$. Figure 18 shows the instantaneous local Nusselt number for the in-line bank. The local Nu is based on an instantaneous local heat transfer coefficient $h = \dot{q}_w/(T_w - T_b)$ and normalized with respect to the long-term, time-average value $\overline{\mathrm{Nu}}$ as defined in equations (16) and (17).

3. DISCUSSION

3.1. Description of the Flow Field

3.1.1. *Rotated-square bank*

Figures 3(a–f) and 4(a–f) show a sequence of velocity vectors and streamlines for the rotated-square tube bank at Re = 300. (a) A clockwise vortex has developed behind the

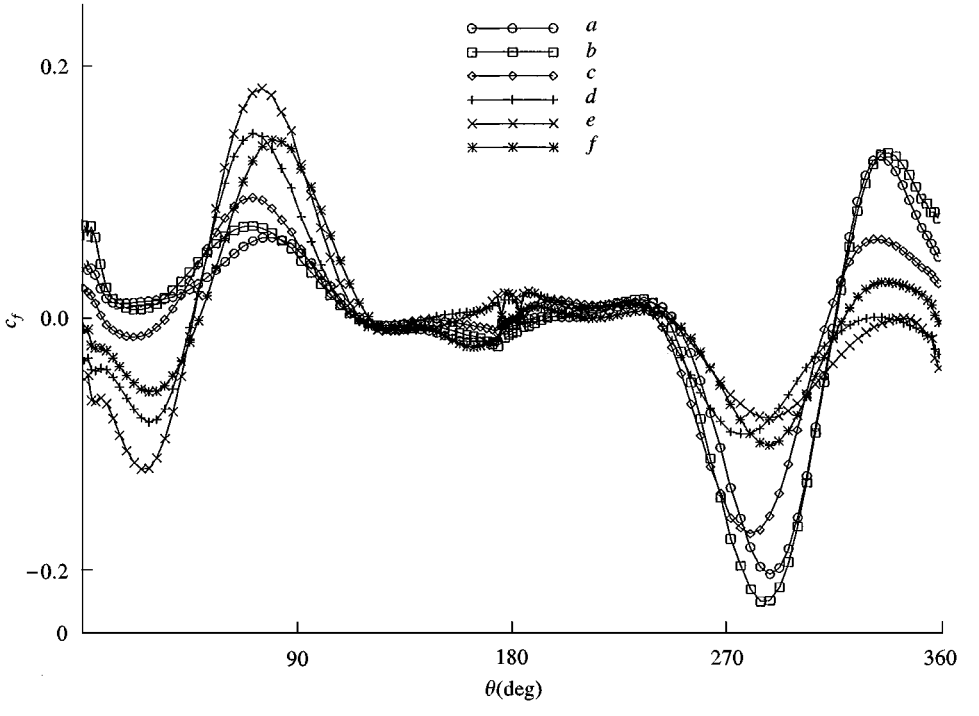

Figure 17. c_f versus θ, for Re = 300, $Sh_0 = 0{\cdot}1$, $V_0 = 0{\cdot}2u_m$; in-line bank.

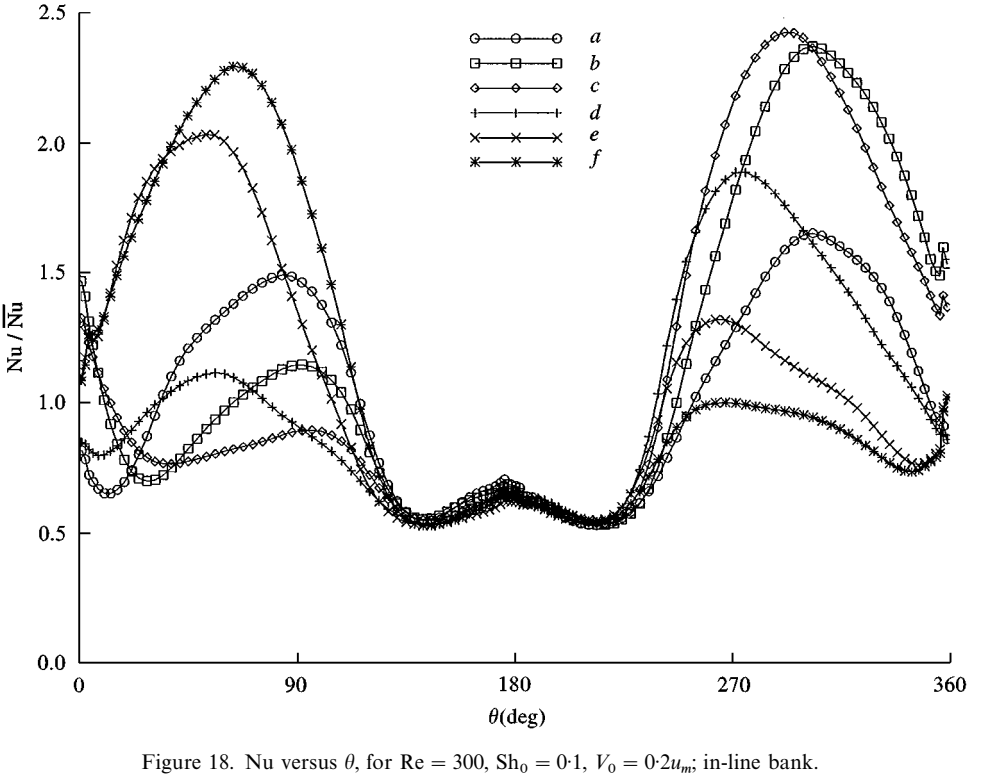

Figure 18. Nu versus θ, for Re = 300, $Sh_0 = 0{\cdot}1$, $V_0 = 0{\cdot}2u_m$; in-line bank.

top-rear side of the upstream cylinder D; below and downstream of this first vortex, a second counterclockwise vortex can also be seen. (b) The clockwise vortex grows in the presence of the favourable shear layer (rate-of-deformation gradient) and increases the angular momentum. (c) This increases the size of the vortex, and displaces it back into the wake, to the rear of cylinder D. As the vortex moves across the centreline, it encounters an adverse shear layer (on the lower side of the cylinder) which entrains it, and decreases the angular momentum. The opposing streams result in the birth of a new counterclockwise vortex at a location between the existing vortex and the main stream below. (d) The clockwise vortex is now displaced downstream, and the new counterclockwise vortex begins to grow in the presence of the favourable shear layer behind the rear-lower side of the cylinder. The clockwise vortex moves along with the flow, and (e) is destroyed as it passes through the minimum cross-section of the subsequent row B-B. By (f) the cycle is complete. The wake behind cylinder D is S-shaped, and switches back and forth in a sinuous fashion because alternate quantities of clockwise and counterclockwise momentum are being imparted. Two rows downstream, the flow bifurcates at a point towards the front of cylinder E. The location of this point moves as the fast-moving free streams stick to alternate sides of cylinder E. This situation results in a Coanda-like effect. The large-scale, symmetry-breaking bifurcation thus represents a fundamentally different solution to the perturbation problem than that obtained from calculations which presume the motion may be treated as one which is steady.

3.1.2. *In-line bank*

Figures 7 and 8 show the transient flow regime for the in-line bank at $\mathrm{Re} = 300$. The motion is similar in many ways, but also different from that in the staggered geometry. The streamline plots in Figure 8 show that a counterclockwise vortex has formed initially in the space between cylinders A and B. This vortex moves into the central inter-tube zone, and thus spawns a small clockwise vortex behind the upstream cylinder, as described above. The new vortex expands to fill the inter-tube region and displaces the original counterclockwise vortex which decays as a result of friction forces. The clockwise vortex fills the entire inter-tube space and detaches from behind the cylinder, and thereby induces the formation of a counterclockwise vortex, and the sequence repeats itself.

Comparison of the vector fields in Figure 3 to those in Figure 7 reveals that the transient motion is much less pronounced for the in-line geometry than for the staggered bank. For the former case, the wake is relatively quiescent because of the shading effect of subsequent rows. Inspection of animation sequences revealed that as each vortex develops, fluid particles near the wall enter the inter-tube zone from the free stream. As the vortex is dissipated downstream, fluid particles are ejected back out into the main stream, so there is momentum exchange between the vortex and the fast-moving free stream. The free stream undulates with the direction of rotation of the vortices, i.e., there is a shear-layer instability. The single attachment point oscillates with the flow. Calculations which presume steady, fully developed periodic flow predict two symmetric reattachment points on either side of the cylinder (Beale & Spalding 1998). For $s/d = 2$, only one vortex is ever fully formed in the inter-tube space, although up to three partially formed vortices of opposite spin may be present for a very short period of time.

3.1.3. *General remarks*

For both in-line and staggered banks, the flow fields were found to be qualitatively similar over a wide Re range. The size of velocity vectors within the vortex increased with Re, even

though the streamline plots were relatively similar, and only minor differences in size of vortices, number present, residence time, etc., were noted over a wide Re range. Comparison of animated sequences of the present results with the 16 mm film clip of Weaver & Abd-Rabbo (1984) revealed the numerical work to be physically realistic, as verified independently by others (Païdoussis 1994). It appears that calculated vortices may survive for a shorter time than did those observed in flow visualization studies, perhaps because of numerical diffusion associated with the spatial hybrid scheme and the use of the first-order temporal discretization in equation (4). Also, no two vortices are precisely the same in nature, whereas the numerical calculations generate a highly repeatable, periodic motion. The curves shown in Figures 4 and 8 are streamlines—not streak lines like those obtained in experimental work. Tests showed that for larger values of s/d the behaviour is more like that of single cylinders, in that several vortices coexist in the wake, in a way consistent with the results of Wallis (1939).

Inspection of Figures 6 and 10 reveals that the formation of the vortices has a significant effect on the temperature field. Consider, for example, Figure 10. As each vortex becomes fully developed, it detaches and occupies the central zone between the two cylinders. At this time, there is a strong cross-flow at the front of the downstream cylinder B. The effect is to pull (cold) fluid at the free-stream temperature in, and across the (hot) downstream cylinder B. This results in a trough in the temperature field near the lower front side of cylinder B [Figure 10(b)]. This sharp temperature gradient quickly collapses as the vortex loses angular speed and is dissipated on the lower front side of cylinder B [Figure 10(c)]. As the subsequent clockwise vortex fills the inter-tube space, another tongue of cold fluid is drawn from the attachment point on the upper side of cylinder B [Figure 10(d, e)]. Thus, there is substantial gross mixing of free-stream and inter-tube fluids due to the alternate swirling motion of the vortices which results in more effective heat transfer.

3.2. Independence of Solution

3.2.1. *Staggered bank*

Inspection of the upstream monitor-point v-values in Figure 11 shows that at Re = 30, the disturbance is damped out. For Re = 100 the transient maintains itself, as is just apparent from the end of the trace in Figure 11 (NB: the downstream response leads by 240 time-steps). As Re is increased, the amplitude of the v-fluctuations increases to approximately $0{\cdot}5u_m$ at Re = 300. At a sufficiently high Re value a definite "transistor" or "triode" effect is observed: small lateral perturbations are amplified under the action of the main flow, so the downstream oscillations are much larger than the upstream disturbance—i.e., there is a fundamental instability to lateral perturbations of the symmetry line. A stable periodic behaviour is eventually established with no gain, by means of a back-substitution process. Figures 12 and 13 show the transient to be relatively unaffected over a wide range by either the frequency f_0 or the magnitude V_0 of the initially applied disturbance. Note that oscillations arose spontaneously with $V_0 = 0$. In fact, for the staggered geometry, spontaneous oscillations arose regardless of whether or not the explicit lateral back-substitution mechanism was invoked. This suggests that these numerical results are a reasonable facsimile of the actual flow within the passages of a rotated square tube bank.

3.2.2. *In-line bank*

For the in-line square bank initially applied, spanwise oscillations were amplified under the action of the main flow, especially at higher Re values, although this effect was less

pronounced than for the rotated square geometry. For Re = 30, no periodic behaviour was observed. At higher Re, the same effect as that described above was noted. For the in-line tube bank, however, the excitation frequency appears to affect the final outcome of the calculations (Figure 14). When the initial frequency f_0 was applied such that $0{\cdot}05 \leq \mathrm{Sh}_0 \leq 0{\cdot}5$, final values of Sh lay in a band between approximately 0·1 and 0·2. At high frequency ($\mathrm{Sh}_0 = 0{\cdot}5$), the response degenerates to a much lower frequency. This suggests that if the calculations were continued for a very long time, the flow may ultimately converge on a natural frequency independent of the initially applied signal. The results of the numerical calculations may not necessarily correspond to the naturally occurring oscillations in an in-line square tube bank, but the downstream response to a stimulated perturbation would be similar to that shown in Figures 7–10. For very widely spaced in-line banks, it was possible to obtain transient behaviour spontaneously. It is believed that the influence of the amplitude is primarily on the number of time-steps required to reach a repeatable periodic behaviour. In experimental work on an in-line square array with $s/d = 1{\cdot}5$, Price *et al.* (1991) noted that the oscillation of the dividing line would build up to a maximum, then decay to a minimum before building up again. This ubiquitous behaviour is consistent with the results of Figure 14, and could indicate the presence of a beat frequency associated with multiple Sh, the effects of large-scale free-stream turbulence, or both.

3.2.3. *General remarks*

The basis for the present method is the application of a harmonic excitation. The iterative feedback mechanism emulates the row-by-row development of the oscillatory response, which would occur in a large-scale heat exchanger. The choice of the initial and boundary conditions may affect some aspects of the process, and limitations of computational resources necessitate calculations be terminated sooner than preferred; however, the results of this study provide interesting and meaningful insight into the complex nature of the flow in the passages of tube banks.

The downstream flow is extremely responsive to any initial excitation if it is applied across the lateral boundary (Figure 1, A-B). Fluctuations applied along the inlet (across a-a') are damped out quickly. When downstream values were back-substituted, it was again the lateral, spanwise terms that were dominant. The streamwise (inflow) values were also important, but subordinate. The calculations suggest that the staggered configuration is fundamentally more prone to transient behaviour than the in-line bank, and that it is easier to generate instabilities for a larger pitch-to-diameter ratio s/d. This result is consistent with experimental flow visualization studies.

Unlike external transient flow past simple bluff bodies, the correct prescription for the boundary conditions is not obvious. Several combinations of initial and boundary conditions were considered prior to those that were adopted here: for example, doubly periodic conditions where $\tau_x = 0$ and $\tau_y = 0$ (Pruitt *et al.* 1990; Stuhmillar *et al.* 1988). Their use resulted in the transient motion being completely damped out, an outcome consistent with the laminar-flow results of Stuhmillar *et al.* (1988).

For the staggered geometry, vortex shedding could be induced passively without the disturbance-feedback mechanism, and a comparison of the results of Tables 2 and 3 reveals broad agreement in performance measures for the most part, regardless of whether the mode of excitation was passive or active. The active excitation method is nevertheless recommended for all geometries: in the absence of an explicit overall lateral-momentum constraint, the flow tends to wander at low Re (residual drift), while overall stability is

difficult to control at high Re. The explicit prescription for lateral momentum is valid, as sources of mass and momentum do emanate from these boundaries: i.e., for a significant fraction of the cycle they are upstream. This prescription is also suitable for steady, fully developed oblique (diagonal) cross-flow. The downstream pressure boundary condition based on potential flow theory is consistent with classical boundary-layer theory and generates a reasonable solution to the flow-field problem. Some local distortion of the pressure field due to the concave shape of velocity profile was observed near the walls, but this does not affect the upstream results significantly. Forward substitution of upstream pressure profiles downstream (Beale & Spalding 1998) is a plausible alternative in theory, but since τ_x is not known *a priori*, it will not correspond to a discrete number of computational time-steps. The impact of the premise that streamwise diffusion is subordinate to convection or inertia at the inlet is small.

Lateral diffusion was accounted for everywhere. For the in-line case, no reverse flow occurred at either the inlet or the outlet. For the staggered geometry, the module used to calculate performance measures was located one-half pitch downstream from the inlet. Whether the assumption that the lateral transients are in phase $\mathbf{u}(x, y + s_y, t) = \mathbf{u}(x, y, t)$, $\tau_y = 0$ is, however, a point for discussion: the alternate vortex-shedding patterns described in this paper are consistent with those observed experimentally; other modes have also been observed however, e.g., symmetric vortex shedding at low Re in a rotated-square array (Price *et al.* 1991) and alternate vortex shedding in an in-line bank with adjacent streams out of phase $f\tau_y = \frac{1}{2}$ (Ziada & Oengören 1992). Attempts to generate the latter behaviour numerically by the construction of two complete modules in the crosswise y direction degenerated to the periodic case $f\tau_y = 0$. Lateral fluctuations can only arise and be propagated in the presence of minor differences in velocity or pressure between adjacent modules, so the argument that both $\mathbf{u}(x, y + s_y, t) = \mathbf{u}(x, y, t)$ and $p(x, y + s_y, t) = p(x, y, t)$ exactly is seemingly paradoxical. Indeed, experimental flow visualization studies reveal that no two vortices are ever precisely the same. Nevertheless, if adjacent modules in both streamwise and crosswise directions were not in phase, the instantaneous bulk velocity would vary from module to module, which suggests the presence of an inherently 3-D (and possibly random) component to the motion.

Beale (1993a) contained comparisons of the results of calculations for steady, fully developed 2-D flow and steady, fully developed 3-D cross-flow in cylinders with diameter d and length l (fin-and-tube heat exchanger). The results suggested that at low Re values the 3-D pressure loss and heat transfer factors differ negligibly from the 2-D cases, provided $l : d \geq 10 : 1$. The results also showed that at higher Re values, complex 3-D flow patterns do in fact arise: in addition to the wake vortices at the back of each cylinder, a downward motion at the front of each cylinder results in a horseshoe vortex. In a staggered bank, these two flow phenomena are located almost side by side, and a complex interaction is observed at a sufficiently high Re value. This interaction may ultimately lead to the breakdown of the steady periodic behaviour and the resulting generation of turbulence. Detailed transient 3-D studies are beyond the scope of this paper; the need for such studies in the future, however, is readily apparent.

Convergence studies revealed some differences in the magnitude of the fluctuating velocity component; however Table 1 also reveals that Sh values obtained on the basis of twice the time-steps and 2·5 times the sweeps per time-step, agreed to within 0·7% (staggered) and 1·3% (in-line). The use of coarser grids was found to damp out the oscillatory behaviour, while the use of grids finer than the 80×160 cells adopted for this study could not be considered because of finite computer limitations. It is worth noting that the in-line grid was orthogonal, whereas the staggered geometry necessitated the construction of a nonorthogonal mesh.

3.3. Pressure Distribution

Observed pressure fields were quite complex (see Figures 5 and 9), and quite different from those observed from potential or steady-viscous flow calculations (Beale & Spalding 1998; Beale 1993a, b). A pressure maximum occurs near the bifurcation point, minima occur at the sides of the cylinder (near $\theta = 90^\circ$), and multiple extrema arise in the inter-tube space.

Within the wake, the u-component oscillates at $2f$ since u varies with the magnitude of the v-fluctuations and influences the pressure trace, which is either at f, $2f$ or a combination, depending on the strength of the two velocity components. The crosswise v-velocity oscillates in a repeatable sinuous fashion, while the magnitude of the streamwise u-fluctuations tends to increase with Re and become erratic, so that by $\mathrm{Re} = 3\,000$ the pressure fluctuations also increase and become erratic and unstable. With streamwise frequency twice the crosswise frequency, Sh based on a wake value of **u** is anisotropic. Several experimental workers (Chen 1978; Fitzpatrick 1986; Price *et al.* 1987; Weaver & Abd-Rabbo 1986; Ziada *et al.* 1989, 1992) have noted the existence of multiple Sh. It is interesting to speculate on the existence of higher harmonics, interference effects or beats, and the influence of the erratic pressure fluctuations on the generation of random free-stream turbulence.

Figure 15 shows $c_p(\theta)$ for the in-line square bank (same sequence of events as in Figure 7). A single pressure maximum is associated with the establishment of the attachment point at the front side of the cylinder. The maximum rises and falls on opposite sides of the cylinder. Further downstream, the pressure minima are also substantially affected by the transient nature of the flow. Significant fluctuations in c_p are observed around the entire periphery of the cylinder. Figure 16 exhibits c_P against θ for the rotated square tube bank (same as in Figure 3). The results are qualitatively similar, although the transient fluctuations in c_P around the periphery are significantly larger than for the in-line square case, which reflects the more vigorous motion. A rise in pressure is again associated with the establishment of the attachment point at one or other side of the front of the cylinder. The pressure minima at the sides of the cylinder fluctuate. Some minor discontinuities at the leading and trailing edges are due to grid-related effects. The presence of an overall favourable pressure gradient in the streamwise direction $\overline{\Delta p}_{\mathrm{row}}/s_x$ would tend to impede vortex formation and suppress such phenomena to higher Re in tube banks than in single cylinders. The pressure field may also assist transience: for potential flow in staggered banks (Beale 1993a, b), there is a checkerboard pressure distribution with global maxima at $\theta = 0$ and 180°, and minima at $\theta = 90$ and 270° on the cylinder wall. A saddle point occurs in the wake region at the next offset row [at the mid-point between D and E, Figure 1(b)], which suggests that a state of metastable equilibrium exists whereby any tendency for lateral wake switching in staggered banks, and jet instabilities in in-line banks, would be reinforced.

3.4. Frequency and Drag

3.4.1. *Staggered bank*

Tables 2 and 3 show that for the staggered tube bank, Sh values ranged between 0·22 and 0·35, with the mean values near 0·3. Žukauskas *et al.* (1988) suggest these to be of the order of 0·34, whereas the Weaver *et al.* (1986) correlation, based on an interpretation of an Owen (1965) hypothesis, indicates a value of $\mathrm{Sh} = 0{\cdot}33$. Comparison of Tables 2 and 3 shows a consistency in Sh values; for actively induced excitation, calculated values range between -21% and $+6\%$ of the value in Owen (1965), while the self-induced values range between -36% and -6%. As Re increases, the mean value of Eu decreases, while the periodic

component becomes substantially larger. At high Re values, the fluctuating component of the pressure field is very large compared to the steady-state value. This affects both Eu and c_D, which become erratic. On the other hand, c_L oscillates in a stable, sinusoidal-like manner. Time-average and fluctuating components of Nu increase with Re, although the latter is a much smaller fraction of the mean value than was observed for Eu or c_D, as indicated by the ratio σ/μ. Tables 2 and 3 reveal agreement to be much better than Eu values when the cases of stimulated and spontaneous vortex shedding are compared: because of the length of time required to make the numerical calculations, only a few cycles were considered in this study. Quantitative measures of performance should therefore be considered as only approximate.

3.4.2. *In-line bank*

Table 4 reveals Sh calculations by the authors ranging from 0·09 at low Re values, to about 0·12 at Re = 1000. Only 6–8 cycles were used to compute these values, and while they should be considered approximate, they are of the same order as the applied disturbance. A variety of experimental data have been gathered on Sh for in-line tube banks. Žukauskas *et al.* (1978) suggest that for $s/d = 2$, Sh = 0·24 at Re = 500. This value is in broad agreement with the values near 0·25–0·26 extrapolated from Weaver *et al.* (1986), Žukauskas *et al.* (1988), and also Chen (1968) and Fitz-Hugh (1973). The latter sets of results are known to be in the acoustic range, and are therefore not considered appropriate for comparison with the present work. Rae & Wharmby (1987) suggest a lower value for Sh, around 0·155, for $s/d = 2$, in the nonacoustic vortex-shedding regime. These lower Sh values were independently validated by Ziada & Oengören (1992) for a $1{\cdot}75 \times 2{\cdot}25$ in-line bank, in the nonacoustic regime. The present authors' values are thus comparable to those of Rae & Wharmby (1987), but are about 20–40% lower. Weaver *et al.* (1986) show the very substantial disparities in measured experimental values of Sh reported by the various authors for $s/d = 1{\cdot}5$ and 2. The disparities are attributed to the presence of multiple Sh.

The amplitude of the lateral v-fluctuations was observed to be quite large: for Re > 300, the peak oscillations can be up to 50% of the bulk streamwise velocity. Above this value, v-fluctuations remained fairly constant, repeatable and sinusoidal-like. The lateral fluctuations tend to be stable at high Re but erratic at low Re, while the converse is true for the streamwise and pressure fluctuations. The magnitude of streamwise u-velocity and pressure fluctuations increased in strength over the entire Re range, with the pressure signal becoming less stable at higher Re. The quantity $f\tau_x$ in Table 4 represents the difference between the upstream and downstream crosswise v-velocity fluctuations, expressed as a fraction of a cycle. It can be seen that the upstream transient precedes the downstream value by between 0·44 and 0·55, i.e., the oscillations are close to a half-cycle (or 180°) out of phase regardless of Re. This trend is consistent with the observations of experimental workers (Weaver & Abd-Rabbo 1985; Ziada & Oengören 1992).

Time-average Eu converged to a value close to the steady-state value in the low Re range (Beale 1993a). As Re increases the mean value decreases, while the periodic component becomes substantially larger. At high Re, the fluctuating component of the pressure field is large compared to the steady-state value: at times, there is even an instantaneously favourable pressure gradient. (The apparent increase in Eu at Re = 3 000 is observed because the simulation is of insufficient length, and the Re range for which free-stream turbulence can be ignored is exceeded.) Oscillations of the lift coefficient were observed to be sinusoidal-like, with the peak c_L value at Re = 1000. Overall, c_D values were observed to decrease with an increase in Re. The fluctuating component of c_D is large compared to the mean value.

Figure 17 shows $c_f(\theta)$ for the in-line bank. The large negative values of c_f between $\theta = 0$ and 45° indicate the strength of the shear-inducing vortices. Values of $c_f = 0$ give the location of the attachment and separation points, one of which is apparent at any given moment, unlike the steady case where there are two of each. These results illustrate the fundamental difference between the results of the calculations performed here, and solutions based on the premise of steady flow (Beale & Spalding 1998). With regard to heat transfer, both time-average and fluctuating components of $\overline{\mathrm{Nu}}$ increase with Re, but the latter is a much smaller fraction of the mean value than was observed for Eu or c_D. Values of $\overline{\mathrm{Nu}}$ are higher than those observed for steady flow as a result of the increased mixing of the fluid. $\overline{\mathrm{Nu}}$ is calculated on the assumption that the upstream bulk fluid temperature is constant: in fact, the bulk temperature also fluctuated at higher Re, but these fluctuations were minor. Figure 18 shows that there is substantial time variation in the local Nusselt number distribution for the in-line geometry. Heat transfer is a global maximum at the front of the cylinder near the attachment point. The heat transfer transient lags slightly behind the shear stress transient. For the staggered bank, the maximum oscillates in a zone towards the front of the tube, unlike the results of steady-state calculations which predict a stationary maximum at $\theta = 0°$.

4. CONCLUSIONS

Both in-line and staggered tube banks exhibit transient behaviour for $\mathrm{Re} > 100$ whereby spanwise perturbations are amplified, while at lower Re they decay. For the in-line geometry, an explicit excitation and feedback mechanism was required to generate a transient, fully developed periodic motion. Vortices were generated and shed from alternate sides of the cylinders. This phenomenon resulted in a shear-layer instability between the wake and the rapidly moving free stream. Only one fully formed vortex was present in the inter-tube space at any given time. The streamwise phase difference was approximately 180°. Only one mode of transient behaviour was observed: when multiple lateral modules were considered, the flow always stabilized to the in-phase condition. Observed Sh were dependent on the initial excitation frequency f_0. The nondimensional numbers Eu, Nu, c_P, c_D and c_L all displayed a strong transient behaviour substantially different from that obtained from numerical calculations for steady-periodic flow. The Euler number Eu and drag coefficient c_D displayed very large fluctuations about the mean, while heat transfer appeared to be enhanced as a result of mixing of the fluid. Both fluid flow and scalar transport in tube banks were substantially affected by transient effects for $\mathrm{Re} \geq 100$. In the case of pressure drop and drag, large fluctuations were observed. Skin friction and heat transfer are also substantially different from the results of numerical calculations for steady, fully developed periodic flow. Strouhal numbers ranged between 0·09 and 0·12, or -20 to -40% below experimental values.

In the staggered tube bank, alternate vortex-shedding and wake-switching effects were observed. These were shown to be essentially independent of the disturbance over a range of applied amplitudes and frequencies; moreover, it was shown that the transients could develop spontaneously. The transient nature of the motion has a large impact on the value of pressure-related quantities such as c_p and Eu. Strouhal numbers were in reasonable agreement with experimental data; for the staggered geometry, Sh values ranged between 0·26 and 0·35, or from -21 to $+6\%$ of measured values.

The nature of the problem is such that the flow-field calculations are influenced by the grid, boundary conditions and numerical scheme. The quantitative results of this numerical experiment should therefore be considered as only approximate, particularly for the in-line

square geometry. Nonetheless, much insight has been gained into the nature of the excitation mechanism and response, and the resultant effects upon transport phenomena within the passages of tube-bank heat exchangers. The main conclusion of this study is that the flow is fundamentally unstable to lateral perturbations. As a result of this triode-like effect, small symmetry-breaking oscillations are amplified and result in large pressure fluctuations acting on the walls of downstream tubes. It is generally accepted now that, other than fluidelastic instabilities, the main causal mechanisms for flow-induced vibrations are vortex shedding, acoustic coupling and turbulent buffeting. One advantage of numerical analysis is that the effects of each of the phenomena may be isolated and investigated independently. Here only the former was considered: a majority of heat exchangers operate at intermediate Re values, where the presence of turbulence in the free-stream passages influences the flow. It is important that future modelling research address the subject of turbulent buffeting, in the regime where the characteristic length of the eddies is large (Owen 1965), since this subject has received little attention to date. It is to be anticipated that future advances in mathematical modelling will lead to more accurate computer-based calculations, which will enhance traditional empirical techniques, and increase knowledge and confidence in the design of heat exchangers.

References

Abd-Rabbo, A. & Weaver, D. S. 1986 A flow visualisation study of flow development in a staggered tube array. *Journal of Sound and Vibration* **106,** 241–256.

Antonopoulos, K. A. 1979 Prediction of flow and heat transfer in rod banks. Ph.D. Thesis, Imperial College, University of London.

Beale, S. B. 1993a Fluid flow and heat transfer in tube banks. Ph.D. Thesis, Imperial College, University of London.

Beale, S. B. 1993b Potential flow in in-line and staggered tube banks. NRC Technical Report IME-CRE-TR-006. National Research Council of Canada, Ottawa, Canada.

Beale, S. B. 1997a Tube banks, crossflow over. In *International Encyclopedia of Heat and Mass Transfer* (eds G. F. Hewitt, G. L. Shires, and Y. V. Polyshaev), pp. 1188–1193. New York: CRC Press Inc.

Beale, S. B. 1997b Tube banks, single-phase heat transfer in. In *International Encyclopedia of Heat and Mass Transfer* (eds G. F. Hewitt, G. L. Shires, and Y. V. Polyshaev), pp. 1188–1193. New York: CRC Press Inc.

Beale, S. B. & Spalding, D. B. 1998 Numerical study of fluid flow and heat transfer in tube Banks with stream-wise periodic boundary conditions. *Transactions of the CSME* **22,** 4, 397–416.

Borthwick, A. 1986 Comparison between two finite-difference schemes for computing the flow around a cylinder. *International Journal for Numerical Methods in Fluids* **6,** 275–290.

Braza, M., Chassaing, P. & Minh, H. H. A. 1986 Numerical study and physical analysis of the pressure and velocity fields in the near wake of a circular cylinder. *Journal of Fluid Mechanics* **165,** 79–130.

Caretto, L. S., Gosman, A. D., Patankar, S. V. & Spalding, D. B. 1972 Two calculation procedures for steady, three-dimensional flows with recirculation. In *Proceedings of the 3rd International Conference on Numerical Methods in Fluid Mechanics*. Lecture Notes in Physics, Vol. **2,** pp. 60–68. Berlin: Springer-Verlag.

Chang, K. S. & Song, C. J. 1990 Interactive vortex shedding from a pair of circular cylinders in a transverse arrangement. *International Journal for Numerical Methods in Fluids* **11,** 317–329.

Chen, S. S. 1978 Crossflow-induced vibrations of heat exchanger tube banks. *Nuclear Engineering and Design* **47,** 67–86.

Chen, Y. N. 1968 Flow-induced vibration and noise in tube-bank heat exchangers due to von Karman streets. *ASME Journal of Engineering for Industry* **90,** 134–146.

Eaton, B. E. 1987 Analysis of laminar vortex shedding behind a circular cylinder by computer-aided flow visualization. *Journal of Fluid Mechanics* **180,** 117–145.

Fitz-Hugh, J. S. 1973 Flow-induced vibration in heat exchangers. In *UKAEA/NPL International Symposium on Vibration in Industry*, Keswick, U.K. Paper No. 427, pp. 1–17.

Fitzpatrick, J. A. 1986 A design guide proposal for avoidance of acoustic resonances in in-line heat exchangers. *ASME Journal of Vibration, Acoustics, Stress and Reliability in Design* **108,** 296–299.

Gresho, P. M., Stevens, T., Lee, R. L., & Upson, C. D. 1984 A modified finite element method for solving the time-dependent, incompressible Navier–Stokes Equations. Part 2: Applications. *International Journal for Numerical Methods in Fluids* **4,** 619–640.

Harlow, F. H., & Welch, J. E. 1965 Numerical calculation of time-dependent viscous incompressible flow of fluid with free surface. *Physics of Fluids* **8,** 2182–2189.

Johnson, A. A., Tezduyar, T. E. & Liou, J. 1993 Numerical simulation of flows past periodic arrays of cylinders. *Computational Mechanics* **11,** 371–383.

Jordan, S. K., & Fromm, J. E. 1972 Oscillatory drag, lift, and torque on a circular cylinder in a uniform flow. *Physics of Fluids* **15,** 371–376.

Lecointe, Y. & Piquet, 1984 On the use of several compact methods for the study of unsteady incompressible viscous flow round a circular cylinder. *Computers and Fluids* **12,** 255–280.

Le Feuvre, R. F. 1973 Laminar and turbulent forced convection processes through in-line tube banks. Ph.D. Thesis, Imperial College, University of London.

Ng, C. W., Cheng, V. S. Y. & Ko, N. W. M. 1997 Numerical study of vortex interactions behind two circular cylinders in bistable flow regime. *Fluid Dynamics Research* **19,** 379–409.

Owen, P. R. 1965 Buffeting excitation of boiler tube vibration. *I.Mech.E. Journal of Mechanical Engineering Science* **7,** 431–439.

Païdoussis, M. P. 1982 A Review of flow-induced vibrations in reactors and reactor components. *Nuclear Engineering and Design* **74,** 31–60.

Païdoussis, M. P. 1994 Personal communication.

Patankar, S. V. 1980 *Numerical Heat Transfer and Fluid Flow*. Hemisphere: New York.

Patankar, S. V., & Spalding, D. B. 1972 A calculation procedure for heat, mass, and momentum transfer in three-dimensional parabolic flows. *International Journal of Heat and Mass Transfer* **15,** 1787–1806.

Polak, D. R. & Weaver, D. S. 1995 Vortex shedding in normal triangular tube arrays. *Journal of Fluids and Structures* **9,** 1–17.

Price, S. J., Païdoussis, M. P., Macdonald, R. & Mark, B. 1987 The flow-induced vibration of a single flexible cylinder in a rotated square array of rigid cylinders with pitch-to-diameter ratio of 2·12. *Journal of Fluids and Structures* **1,** 359–378.

Price, S. J., Païdoussis, M. P., Mureithi, W. N. & Mark, B. 1991 Flow visualization in a 1·5 pitch-to-diameter rotated square array of cylinders subject to cross-flow. In *Flow Induced Vibrations*, Vol. 1, pp. 243–252, London: I.Mech.E.

Pruitt, J. M., Hassan, Y. A., & Steininger, D. A. 1990 Large eddy simulation of turbulent flow in a tube bundle. Paper presented at the *Winter Annual Meeting of the ASME*, Dallas, TX, U.S.A.

Rae, G. J. & Wharmby, J. S. 1987 Strouhal numbers for in-line tube arrays. In *Proceedings of International Conference on Flow-induced Vibrations*, Bowness-on-Windermere, U.K., pp. 233–242.

Sa, J-Y., & Chang, K-S. 1991 Shedding patterns of the near-wake vortices behind a circular cylinder. *International Journal for Numerical Methods in Fluids* **12,** 463–474.

Spalding, D. B. 1972 A novel finite-difference formulation for differential expressions involving both first and second derivatives. *International Journal for Numerical Methods in Engineering* **4,** 551–559.

Spalding, D. B. 1980 Mathematical modelling of fluid-mechanics, heat-transfer and chemical-reaction processes: a lecture course. HTS/80/1, Computational Fluid Dynamics Unit, Imperial College, University of London.

Spalding, D. B. 1981a Methods of calculating heat transfer within the passages of heat exchangers. HTS/81/4, CFDU, Imperial College, University of London.

Spalding, D. B. 1981b The calculation of heat-exchanger performance. HTS/81/5, CFDU, Imperial College, University of London.

Spalding, D. B. 1982 Four lectures on the PHOENICS Code. CFD/82/5, Computational Fluid Dynamics Unit, Imperial College, University of London.

Spalding, D. B. 1984 PHOENICS 1984 A multi-dimensional multi-phase general-purpose computer simulator for fluid flow, heat transfer and combustion. CFD/84/18, Computational Fluid Dynamics Unit, Imperial College, University of London.

Stuhmillar, J. H., Chilukuri, R., Masiello, P. J., Chan, R. K. C., Yu, J. H. Y., & Ho, K. H. H. 1988 Prediction of localized flow velocities and turbulence in a PWR steam generator. Project S310–14, Final Report, Electric Power Research Institute, Palo Alto, CA (EPRI NP-5555).

Torikoshi, K., Xi, G., Kawabat, K. & Suzuki, K. 1995 Numerical analysis of unsteady flow and heat transfer around bodies by making use of a compund grid system. *Proceedings of* 4*th ASME/JSME Thermal Engineering Joint Conference*, Hawai, pp. 381–398.

Wallis, R. P. 1939 Photographic Study of Fluid Flow between Banks of Tubes. *Engineering* **148,** 423–425; also *Proceedings of the I.Mech.E.* **142,** 379–387).
Watson, V., Walatka, P. P., Bancroft, G., Plessel, T., & Merritt, F. 1990 Visualization of Fluid Dynamics at NASA Ames. *Computing Systems in Engineering* **1,** 333–340.
Weaver, D. S., & Abd-Rabbo, A. 1984 Flow visualization in in-line and staggered tube banks. 16mm ciné-film. Department of Mechanical Engineering, McMaster University, Hamilton, Ont, Canada.
Weaver, D. S. & Abd-Rabbo, A. 1985 A flow visualization study of a square array of tubes in water crossflow. *ASME Journal of Fluids Engineering* **107,** 354–363.
Weaver, D. S. & Abd-Rabbo, A. 1986 A Flow visualization study in flow development in a staggered tube array. *Journal of Sound and Vibration* **106,** 241–256.
Weaver, D. S., Fitzpatrick, J. A. & Elkashlan, M. 1986 Strouhal numbers for heat exchanger tube arrays in cross flow. In *Flow-Induced Vibrations*, 1986 (eds S. S. Chen, J. C. Simonis and Y. S. Shin), pp. 193–200. New York: ASME.
Ziada, S., Oengören, A. & Bülmann, E. T. 1989 On acoustical resonance in tube arrays Part 1: Vorticity shedding. *Journal of Fluids and Structures* **3,** 293–314.
Ziada, S. & Oengören, A. 1992 Vorticity shedding and acoustic resonance in an in-line tube bundle Part 1: Vorticity shedding. *Journal of Fluids and Structures* **6,** 271–292.
Žukauskas, A. A. & Katinas, V. 1988. Flow-induced vibration in heat-exchanger tube banks. *Proceedings IUTAM-IAHR Symposium on Practical Experiences with Flow-induced Vibrations*, Karlsruhe, 1979, pp. 188–196. Berlin: Springer-Verlag.
Žukauskas, A. A., Ulinskas, R. V., Bubelis, E. S. & Sipavičius, C. 1978 Heat transfer from a tube bundle in crossflow at low Reynolds number. *Heat Transfer- Soviet Research* **10,** 9–15.
Žukauskas, A. A., Ulinskas, R. V., & Katinas, V. 1988 *Fluid Dynamics and Flow-Induced Vibrations of Tube Banks*. New York: Hemisphere (English-edition editor: J. Karni).

APPENDIX: NOMENCLATURE

a_P, a_W, a_E, a_S, a_N, a_T	linking coefficients in equation (4)
A	area
c_D	drag coefficient, defined in equation (14)
c_L	lift coefficient, defined in equation (15)
c_f	skin friction coefficient, $= \tau_w/\frac{1}{2}\rho u_m^2$
c_p	specific heat
c_p	pressure coefficient, defined in equation (18)
C	source-term coefficient, defined in equation (5)
d	tube diameter
Eu	Euler number, $= \Delta\bar{p}_{\text{row}}/\frac{1}{2}\rho u_m^2$
f	frequency
f_0	initial frequency
h	instantaneous local heat-transfer coefficient
$\bar{h}$	instantaneous overall heat-transfer coefficient, defined in equation (17)
i	enthalpy
k	thermal conductivity
l	tube length
$\dot{m}$	mass flux, convection flux, $= \rho A u$
Nu	instantaneous local Nusselt number, $= \bar{h}d/k$
$\overline{\text{Nu}}$	time average overall Nusselt number, $= \bar{h}d/k$
p	pressure
$\bar{p}$	time-average pressure
p'	fluctuating component of pressure
p_P	pressure at cell P
$\Delta\bar{p}_{\text{row}}$	time average pressure drop across adjacent rows, defined in equation (8)
p_∞	discharge pressure
$\dot{q}_w$	wall heat flux
Re	Reynolds number, $= \rho u_m d/\mu$
s	pitch
s_x	streamwise pitch
s_y	crosswise pitch

S	source term in scalar equation, equation (3)
S_P	source term in finite-volume equation, equation (4)
Sh	Strouhal number, $= fd/u_m$
t	time
T	temperature
T_b	instantaneous bulk temperature, defined in equation (12)
$\overline{T}_b$	time-average bulk temperature
$\Delta\overline{T}_b$	time-average bulk temperature change across adjacent rows
T_w	wall temperature
$\mathbf{u}$	velocity vector
u	streamwise velocity
u_m	interstitial bulk velocity, at minimum cross-section
U_m	superficial bulk velocity if tubes not present, $= u_m(s_y - d)/s_y$
v	crosswise velocity
v_{mon}	crosswise velocity at monitor-point location
V	source-term value, defined in equation (5)
V_0	peak applied disturbance
x	streamwise displacement
y	crosswise displacement
Γ	exchange coefficient in equation (3)
θ	angle from front of cylinder
μ	sample mean (Tables 2–4)
μ	dynamic viscosity
ρ	density
σ	population standard deviation (Tables 2–4)
τ_w	wall shear stress, $= \mu\partial u/\partial n$
τ_x	streamwise phase
τ_y	crosswise phase
ϕ	general scalar variable in equation (3)
ϕ_P	value of variable ϕ at cell P in equation (4)
ϕ_E, ϕ_W, ϕ_S, ϕ_N	values of variable ϕ at neighbours of P in equation (4)
ϕ_T	value of variable ϕ at cell P at previous time-step